

Received November 17, 2020, accepted December 7, 2020, date of publication December 24, 2020, date of current version January 6, 2021.

Digital Object Identifier 10.1109/ACCESS.2020.3047156

# Review of Flux Interaction of Differently Aligned Magnetic Fields in Inductors and Transformers

JONAS PFEIFFER<sup>1</sup>, (Member, IEEE), PIERRE KÜSTER<sup>1</sup>, ILKA E. M. SCHULZ<sup>2</sup>,  
JENS FRIEBE<sup>1,2</sup>, (Member, IEEE), AND PETER ZACHARIAS<sup>1</sup>, (Member, IEEE)

<sup>1</sup>Department of Electrical Power Engineering, University of Kassel, 34121 Kassel, Germany

<sup>2</sup>Institute for Drive Systems and Power Electronics, Gottfried Wilhelm Leibniz Universität Hannover, 30167 Hannover, Germany

Corresponding authors: Jens Friebe (friebe@ial.uni-hannover.de) and Jonas Pfeiffer (jonas.pfeiffer@uni-kassel.de)

This work was supported in part by the German Federal Ministry of Education and Research (BMBF) through the BMBF Project under Grant 16EMO0234, in part by the Ministry of Science and Culture of Lower Saxony, in part by the Volkswagen Foundation, and in part by the Gottfried Wilhelm Leibniz Universität Hannover through the Open Access Publishing Fund.

**ABSTRACT** Magnetic devices are used in the majority of power electronic applications, e. g. power electronic converters, mains filters or burst/surge protection. Typically, they are the bulkiest and most cost-intensive components. Flux interaction of differently aligned magnetic fields in inductors and transformers can be one opportunity for size and cost reduction. It enables controllable magnetic devices through an additional manipulated variable to improve application design. The presented article gives an overview about different methods of flux interaction of magnetic fields, their background, potentials and open research questions. The focus lies on electrically controlled magnetic devices, realized by auxiliary windings wound on or introduced into the magnetic core to control its saturation and the inductive behavior of the device by injecting a current. However, the given methods and explanations are transferable to magnetic devices influenced by permanent magnets. The background of the different flux interaction methods are explained theoretically and verified by simulations and several laboratory prototypes. The focus of the simulations and experimental investigations lies on magnetic devices for power electronic converters, whereby especially ferrite core materials were used.

**INDEX TERMS** Controllable magnetics, inductor, magnetic fields, flux interaction, transformer.


## I. INTRODUCTION

Magnetic devices have a multifarious scope of application. Especially in the field of power electronic applications, the design of magnetic devices is a significant factor with regard to the application's characteristics such as volume or weight, efficiency and costs. An additional degree of freedom is gained by using flux interaction of differently aligned magnetic fields in magnetic devices over the course of their design process. This enables an enormous improvement potential, especially regarding volume or weight reduction of the device. An example of an improved DC inductor through flux interaction of oppositely aligned magnetic fields using a permanent magnet is given in [1].

The effects of flux interaction of magnetic fields become controllable if the permanent magnet is moved towards a current-carrying auxiliary winding, which is wound on or introduced into the magnetic core. In this way, an additional

magnetic field is generated that results in an additional magnetic flux within the core. An additional oppositely aligned magnetic flux counters the main flux or even cancel it out. Orthogonally aligned magnetic fields and fluxes theoretically do not affect each other, according to the superposition principle. Nevertheless, they can be used to saturate parts of the core, what influences the inductive behavior of the magnetic device, making it adjustable over either its full operation range or parts thereof.

At the moment, the potential of the flux interaction under discussion is not yet clearly summarized. Furthermore, the application of the effect is not, or only rudimentarily, described in the literature. Especially with regards to the great importance of power electronic systems in electrical energy distribution and the necessity to use as many improvement possibilities as possible, especially in the field of magnetic components, the subject area of flux interaction can contain various potentials. The following manuscript is intended to address this and to discuss the subject area in a summarized and clear manner, but also in sufficient scientific depth. For

The associate editor coordinating the review of this manuscript and approving it for publication was Mohsin Jamil .

this purpose, systematic differentiations of flux interaction will be introduced and the interrelationships and effects will be shown by means of analytical and numerical investigations and also measurements.

This manuscript deals with the topic of superposition of differently oriented magnetic fields. It is structured as follows. After the introductory chapter, a differentiation of the possible superpositions of magnetic fields is made and explained in detail in the second chapter “Systematization”. For this purpose, an extensive list of available literature was compiled and discussed according to the systematization. This chapter is intended to provide an easy introduction to the subject area, even for readers from other fields. The third chapter deals with the basic mathematical descriptions of the interactions of magnetic fields, introduces definitions and also deals with relevant assumptions that can be made for simplification. To verify the mathematical basics and to simplify the presentation of basic relationships, results of numerical simulations are presented and summarized in the fourth chapter. The fifth chapter deals with test setups and measurement results of all three introduced classes of superposition of magnetic fields. In the sixth chapter, potentials and further research questions are listed and discussed. All chapters contain a short summary at the end of the chapter. Additionally, the seventh chapter concludes the manuscript with a summary.

## II. SYSTEMATIZATION

According to [2], there are three different methods of superposing magnetic fields in inductors and transformers. They differ in terms of the auxiliary winding’s design, which is either wound on the magnetic core or introduced into it through drill holes. If the auxiliary winding is energized by a current, the resulting additional magnetic flux will saturate parts of the core. This has an effect on the core’s overall reluctance and leads to an adjustable inductance value and a controllable reactance of the magnetic device. The three different methods are presented below:

- parallel biasing
- mixed biasing
- orthogonal biasing

It is important to mention that the allocation to one of the three categories named above is based on the directions of the magnetic fields in the main area of parts of the core e.g. its legs or yokes. Within the transition areas of the magnetic core geometry, e.g. from the center leg to the yoke, the alignment of the magnetic fields might deviate from the allocated category.

### A. PARALLEL BIASING

The usage of permanent magnets in inductors for power electronic converters is investigated and discussed in [3].

As well as using a permanent magnet introduced into the core, the inductance of a magnetic device can be changed by an additional auxiliary bias winding which is wound on

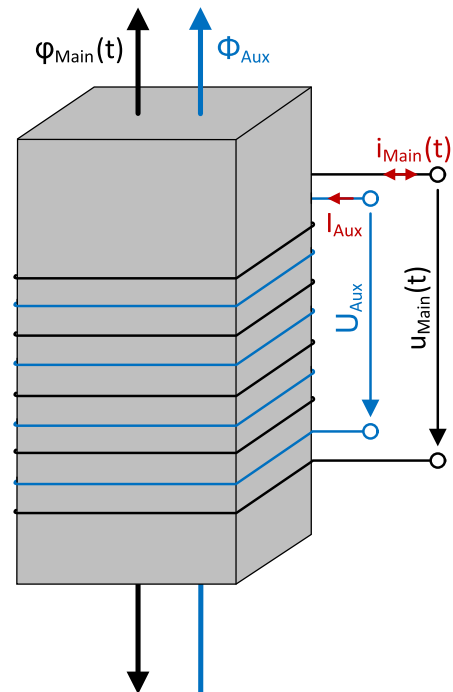


**FIGURE 1.** Core section with main winding and additional auxiliary DC bias winding [2].

the core. The generated auxiliary magnetic flux is parallel to the main flux and either aligned in the same or opposite direction. An example of parallel biasing of a magnetic core section is shown in Fig. 1.

The usage of an auxiliary winding instead of a permanent magnet has the advantage of an adjustable auxiliary current, which generates an adjustable auxiliary magnetic flux within the core material. The result is a controllable reluctance of the magnetic core, which can be adapted to and, more importantly, changed with the device’s operating point. Depending on the characteristic of the magnetic device, significant reluctance changes could be reached with small auxiliary currents.

Furthermore, permanent magnets run the risk of demagnetizing, e.g. through heat or vibration. Especially the latter reason could be critical considering automotive applications. Also an oppositely aligned high flux pulse generated by high current pulses in the main winding is critical because the permanent magnet can be magnetized in its opposite direction. This case could occur e.g. in a fault situation of the application. An additional auxiliary winding is not negatively affected by the abovementioned influences.

Another advantage can be a simpler and more cost-effective manufacture of the magnetic device, especially, if the auxiliary winding replaces a permanent magnet based on rare-earth materials. However, a possible cost advantage does highly depend on the specification of the magnetic device, its characteristic and its manufacturing process.

A disadvantage of using an additional auxiliary winding instead of a permanent magnet is the coupling between main winding and auxiliary winding. Especially if an alternating

current is injected in the main winding, a current ripple in the auxiliary bias winding can be induced. The current ripple can lead to voltage drops over the auxiliary winding, what in turn affects the main winding. Filtering measures in both windings are necessary to suppress unwanted AC ripples and ensure faultless operation under biasing.

A further disadvantage lies in the additional circuit which is needed to provide the required bias current flowing through the auxiliary winding. The implementation of the circuit reduces both power density and overall efficiency of the application. Considering small magnetic devices, the placement of the auxiliary winding can be problematic, as there is a very limited space on the core. A permanent magnet, however, can be introduced into the core without any influence on the winding area. Further investigations are discussed in [3].

Main winding and auxiliary winding have not necessarily to be placed on the same core section. If they are placed on, e. g., different limbs, the coupling and the induction between both windings is reduced. The results are lower voltage drops, hence less filtering requirements are needed. However, a reduced coupling leads to a weaker influence of the bias flux on the main flux. This means that a higher auxiliary current is needed to achieve the desired change of the magnetic device's reluctance.

A detailed review of variable inductors and transformers using parallel biasing is given in [4].

Although the fundamental principle and effects of flux interaction of oppositely aligned magnetic fields has been known for a long time, [5] is one of the first IEEE publications, which makes parallel biasing a subject of discussion. In this article, the flux interaction method is used in a magnetic amplifier for radio telephone transmission. An additional auxiliary DC bias winding is wound on an AC inductor. The DC bias is used to saturate parts of the core and thereby influence its permeability to reduce the inductance of the inductor to the value it would have if the coil included only air.

According to [6], magnetic amplifiers, also known as transductors, were primarily used for long-range radio transmitting stations during World War I and especially in the German military equipment during World War II. After its end, several investigations on transductors were made. Examples are given in [7]–[15]. A typical design of a magnetic amplifier is shown in Fig. 2.

References [7] and [8] deal with fundamental investigations of magnetic amplifiers. Their basic operating principle and common circuits for their application are discussed and proved by measurements. Besides the configurations of EE, EI or U cores, toroidal cores are chosen in the design process, especially if high performance is paramount. Toroidal cores have some advantages regarding manufacturing. However, they are unsuitable if air gaps within the core are essential.

Analytical calculation and modeling methods for transductor design with external and self feedback are presented

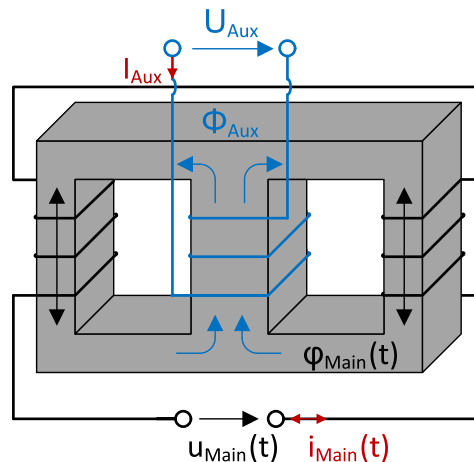


FIGURE 2. A magnetic amplifier [7].

in [9] and [10]. Using a feedback method reduces the needed auxiliary direct current to saturate the magnetic cores.

A few application examples of magnetic amplifiers are given in [11]–[13] to illustrate their widespread use and significance towards comparable technologies, e. g. vacuum tube amplifiers.

In [14] and [15], control strategies for magnetic amplifiers are presented. An additional circuit is used to control the magnetization curve.

Nowadays, magnetic amplifiers are almost completely replaced by semiconductor devices. However, there are still some application fields left where transductors are used because of their high robustness and reliability.

Since the 1980s, parallel biasing is used for low-power high-frequency applications. One of the first IEEE publications for this area of application is given in [16]. In this conference paper, the flux interaction method in conjunction with investigations on air gap design is used to develop a coupled-inductor Cuk converter.

In [17], an E core with a main AC winding on the center limb and two auxiliary DC bias windings on the outer limbs is used to create a variable inductor for high-frequency resonant mode systems. The investigated prototype is designed around commercially available cores. In contrast to transductors, the auxiliary bias winding is usually wound on the outer legs of the magnetic core while the main winding is wound on the center limb.

Especially during the last decade, many investigations on parallel biasing were made, e. g. to reduce the size of the magnetic core or to improve its geometry, as it is shown in [18] and [19]. References [20] and [21] present investigations on magnetic flux optimization in variable inductors. The auxiliary bias winding is not on the main EE core geometry but applied on an additional E core, which is stacked under the main core. The auxiliary bias current does not affect the whole EE core but only its bottom yoke. Thereby, the coupling between main winding and auxiliary bias winding and with that operational asymmetries, which would lead to magnetic flux interactions, are reduced or even canceled.

Parallel biasing cannot only be used to create variable inductors. The principle is transferable to transformer applications, as it is shown in [22].

Several methods for calculation, analytical approximation and modeling of parallel biasing controlled magnetic devices are given in [23]–[34].

References [23]–[27] deal with the analysis of electromagnetic properties and the behavior of the core material as well as with a detailed loss calculation and finite element analysis.

Analyses of controllable magnetic devices using parallel biasing in resonant tanks are presented and discussed in [28] and [29]. The theoretical work is proven by calculation and simulation using MATLAB/SIMULINK or PSIM as well as by experimental results. Comparable investigations are made for grid-tied converter applications in [30].

A precise option to model and calculate magnetic devices controlled by parallel biasing is to simulate their electric or magnetic equivalent circuit. This approach leads to a detailed understanding of the magnetic processes within the device. There are several suitable simulation software programs which can be used. A widespread standard is for equivalent circuit simulation is SPICE. In [31]–[34], several SPICE models for variable inductors in different applications are presented.

Considering parallel biasing in low-power high-frequency applications, a large field of use includes circuits for lamp or LED supply and their control. Examples are given in [35]–[39]. The functional principle can be generalized to similar electronic ballasts, as it is presented in [40]–[44]. Another field of application for controllable magnetic devices covers resonant converters. Due to the adjustable inductance value of the inductor or transformer, the resonant tank can be controlled with an additional variable besides the switching frequency. Therefore, it can be possible to reduce the frequency range of the resonant converter or it might be even operable at constant frequency. Another possibility is to use the additional degree of freedom to reduce reactive power losses, if load conditions change. References [45]–[51] show a few examples of resonant converters using parallel biasing to vary the mounted magnetic devices. However, parallel biasing can also be used in non-resonant converters. In [52]–[58], several examples for different DC/DC converter topologies using controllable inductors and transformers are presented. The objectives of the conducted investigations usually are a substantial volume and weight reduction of the magnetic device or a reduction of the switching losses by achieving zero-voltage switching. A similar objective for a AC/DC converter is presented in [59]. It has to be considered that an additional current source is needed, if active parallel biasing is used. This leads to an additional effort regarding overall volume, weight and efficiency. Reference [60] shows an investigation of using parallel biasing for wireless power transfer in high-frequency resonant circuits.

A few of the investigated applications led to patents. Examples of patented controlled inductors are given in [61]–[63].

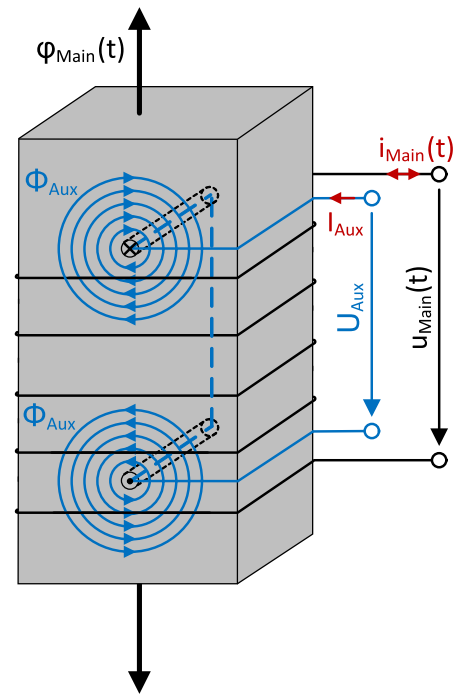


**FIGURE 3.** Core section with main winding and auxiliary DC bias winding introduced to the core through drill holes orthogonal to the main flux [2].

Using parallel biasing to gain a variable inductance value of the magnetic device enables a more complex control strategy which should not be underestimated. Several control strategies and their implementation for different applications are presented in [64]–[70].

## B. MIXED BIASING

Another biasing method is mixed biasing. As it is shown in Fig. 3, the auxiliary bias winding is not wound on the core but introduced into the core material through drill holes, which are orthogonal to the main flux.

The generated auxiliary magnetic field and its magnetic flux are either orthogonal or parallel to the main flux depending on the position of the considered section around the drill hole. Regarding the parallelly aligned sections, the auxiliary bias flux is either aligned in the same or opposite direction. Therefore, the auxiliary bias flux enforces the main flux on the area where both flow in equal direction and lowers it on the area where they are differently aligned.

Introducing an auxiliary bias current into the core material has the effect of saturating a small area around the drill holes which lowers the local permeability. This leads to a virtual air gap (VAG), whereby the overall core's reluctance becomes controllable. The technique of VAG and the resulting virtual air gap variable reactor (VAG-VR) is investigated and discussed in [71].

Regarding the manufacturing process of the drill holes, the mechanical properties of the core material have to be considered. Manufacturing laminated iron cores for low-frequency applications is different to ferrite or iron powder cores for high-frequency applications. Especially ferrite is

critical because of its brittleness, which is similar to ceramics. Therefore, it is recommended to leave the drill process to be performed by ferrite core manufactures or specialized companies what increases the cost of the magnetic core. Another more cost-efficient option might be to integrate the holes during the pressing process of the ferrite core. The use of a modified pressing tool might be profitable if the number of magnetic cores is high enough.

In comparison to transducers, VAG is a relative new technology. Reference [72] is one of the oldest IEEE publications which has been presented close to the 2000s. It contains useful information regarding the arrangement of the drill holes in principle to prevent magnetic fluxes through the whole core. The conducted investigations were continued and expanded in [73]. Especially magnetic flux and permeability simulations were made to explain the electromagnetic processes within the core. Reference [74] deals with the scaling of the VAG-VR to applications with higher voltages and larger power. Similar investigations are made in [75] with the difference that rectangular holes are used.

Calculating the exact VAG length can be difficult. Simulation programs using finite element method are able to support the modeling of the magnetic device. Several publications which deals with the computation of VAG lengths in controllable transformers are presented in [76]–[78]. Improved computing methods regarding accuracy and calculation speed are investigated in [79] and [80]. Reference [81] transmits the VAG principle to toroidal cores. Simulations of the changed main magnetic flux are made to prove the calculation results.

Due to the short period of time where VAG is in use, there are only a few publications presenting applications for that special type of flux interaction method. In [82]–[84], it is used for microgrid tieline reconnection and fail safe operations. A prototype was designed and investigated regarding principle functionality and power losses within the magnetic device. Reference [85] presents a voltage control using a VAG-VR in a developed shunt compensation reactor. The design of the VAG-VR and its control strategy is described in the article. Another application, which is given in [86], shows a coupled transformer with a VAG for dynamic voltage restorers protection. The investigated design avoids drill holes in the core material by using an extended core geometry.

In spite of few scientific application publications, there exist several patents for magnetic devices using VAG which cover basic designs of the technology. Examples are given in [87]–[89]. Attention should be paid to the developed solutions regarding the manufacturing process of the magnetic devices.

Similar to parallel biasing, a control structure for mixed biasing is needed. A simple control strategy for a VAG-VR to achieve harmonic mitigation is presented in [90] and [91]. In both papers, a current modulation together with a full bridge DC/DC converter is used to adjust the control current.

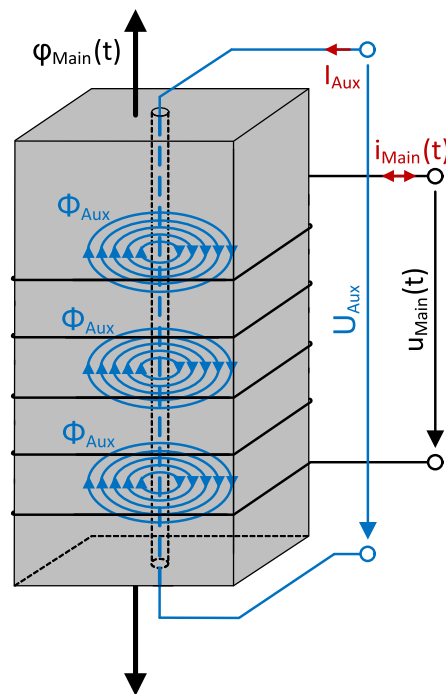


FIGURE 4. Core section with main winding and auxiliary DC bias winding introduced to the core through drill holes parallel to the main flux [2].

### C. ORTHOGONAL BIASING

From the mathematical point of view, the simplest superposition method of differently aligned magnetic fields is orthogonal biasing. It can be described as a special form of VAG, as it is done in Fig. 4 to explain its mode of action. In contrast to mixed biasing, the auxiliary winding is introduced parallel to the main flux. The auxiliary magnetic field and its occurring magnetic flux is always orthogonally aligned to the main flux.

According to the superposition principle, both magnetic fields and fluxes should not affect each other. The coupling between both coils should theoretically be zero, whereby mathematical description and calculations become significantly simpler. In practice, influences from one coil to the other can be observed. These effects are taken up and discussed in Sec. V.

Using orthogonal biasing as a special form of VAG leads to the same challenges regarding manufacturing processes. Furthermore, it has to be checked if this flux interaction method is suitable, especially for laminated iron cores in lower-frequency applications. If the generated auxiliary magnetic flux has to pass the small air gaps between the single iron sheets, the resulting air gap is usually too large, so that orthogonal biasing would not have any effect on the magnetic device.

Although the manufacturing process is similar to VAG, the observed effects on the magnetic device are different. By using orthogonal biasing, other sections of the magnetic core will be saturated in a different way than for parallel biasing. That results in a varied curve progression of the differential inductance value which leads to a modified behavior

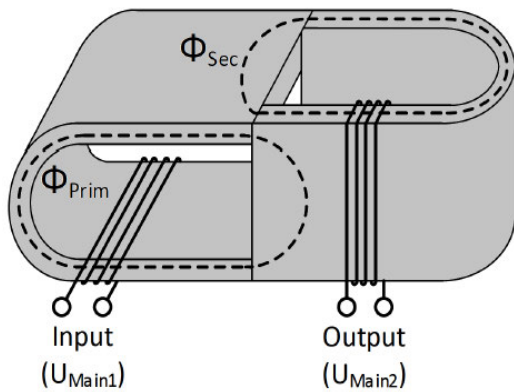


FIGURE 5. A parametric transformer [93].

of the magnetic device. Further discussions will be presented in Sec. IV and Sec. V.

Another significant older way to generate orthogonal biasing is the parametric transformer or paraformer. As it is shown in Fig. 5, the design consists of two wound U cores, one being turned at 90 degrees. It can be seen as a special form of a transformer with practically no mutual inductance and no coupling between the coils. The power transfer occurs through a variation of the magnetic device’s characteristics achieved by saturating the core material. The secondary side works as a parametric oscillator. A detailed analysis of the paraformer is presented in [92].

References [93]–[95] present the basic functional principle of parametric transformers and an analysis. Different construction forms are investigated and discussed in [96]. Considering this article, it can be seen that the design is allocated to orthogonal biasing. Even if the magnetic fluxes within the transition area of the two U cores are not exclusively orthogonally aligned, the arrangement of both windings allows an allocation in this category. An improved structure using drill holes within the magnetic core is shown in [97]. A detailed flux analysis using finite element method to achieve a superconducting controllable reactor is presented in [98].

For a better understanding and an easier calculation and design process, several publications regarding analysis, device characterization and parametric transformer modelling are given in [99]–[104]. An improved and more complex structure of the paraformer is introduced, investigated and discussed in [105] and [106].

Examples for applications of the parametric transformers are given in [107]–[113]. In [107], the device is used to connect two live busbars. Because of the device structure, it is possible to shift power from one bar to another one by adjusting a phase shift angle between the two busbar voltages. The behavior of the paraformer, when it is controlled by thyristors, is shown in [108]. References [109]–[112] present several investigations around AC applications e. g. as a control device for electric motors or a power stabilizer. Further AC applications, can be a DC/AC converter using a parametric transformer. Another improved paraformer design, the cross

transformer, is investigated and discussed in [113]. Several application areas are presented in the article.

For all applications, control strategies for the parametric transformer are essential which take its nonlinear characteristics into account. A fundamental analysis of the paraformer’s control characteristic is shown in [114]. Reference [115] presents a complete and realizable control strategy using a buck-boost DC/DC converter with a simple switch control circuit.

D. SUMMARY

Flux interaction of differently aligned magnetic fields can be achieved either passively by introducing permanent magnets into the core or actively by using an auxiliary bias current. The needed current flows through auxiliary bias windings which are wound on or introduced into the core material. The resulting auxiliary magnetic field affects the core’s overall reluctance. The magnetic devices become controllable, thus gaining an additional degree of freedom regarding the device’s design process.

There are three methods of flux interaction of differently aligned magnetic fields by using an auxiliary current:

The first one is named **parallel biasing**. A second winding, which is wound on the core, generates an auxiliary magnetic flux that is aligned in the same or opposite direction and enforces or weakens the main flux. The effect is similar to the usage of a permanent magnet. This method is used for the magnetic amplifier and bias-controlled magnetic devices.

The second method is named **mixed biasing**. The auxiliary current winding is introduced into the core through drill holes. The resulting auxiliary magnetic field is either orthogonal or parallel to the main field. Thereby, core sections around the drill holes saturate and behave like an air gap. The VAG-VR makes use of this method.

The name of the third method is **orthogonal biasing**. The auxiliary bias winding is aligned in such a way that its magnetic field is orthogonal to the main field. This method can be achieved using a special form of the VAG technique. Another application is the parametric transformer.

An overview of the three biasing methods, their features and their applications is given in Tab. 1.

TABLE 1. Overview of the biasing methods.

Method	Features & Applications
Parallel	Magnetic amplifiers (transducers), bias-controlled magnetic devices, premagnetization for larger usable flux density range
Mixed	Virtual air gap, virtual air gap variable reactor, harmonic mitigation
Orthogonal	Parametric transformers (paraformers), controllable reactors

III. EXPLANATION AND MATHEMATICAL BACKGROUND

A. GENERAL FLUX INTERACTION AND WHY IT OCCURS

It is commonly known that an inductance’s electrical behavior follows  $u = \frac{\partial}{\partial t} (l(t) \cdot i(t))$ . While the secant inductance

$l(t) = \frac{N\phi}{i}$  as well as the differential inductance  $l_d = \frac{dN\phi}{di}$  is usually time-invariant, it can be affected by the inductance itself or by other components in the magnetic circuit if they shift the point of operation to or within the material's nonlinear area of operation, usually near saturation. Such other components in the same magnetic network are generally magnetic sources, meaning current-carrying coils or permanent magnets. In order to derive an assembly's quantitative behavior, the magnetic core must be modeled as a magnetic network, whose passive components and permanent magnets are solely determined by geometry, material and previous state, and possesses the state variables magnetomotive force (MMF)  $f$  and flux  $\phi$ . The electrical state variables of any attached coils can then be expressed as:

$$u = N \frac{d\phi}{dt}; \quad i = \frac{1}{N}f \quad (1)$$

Fluxes or MMFs created by different sources can generally interact when sharing a common region in space of interaction (RSI) within the magnetic core, where it is important to distinguish between (anti-)parallel, orthogonal and mixed interaction (see Sec. II). Any kind of (anti-)parallel fluxes can easily be represented within magnetic network models where several sources (e. g. coils or permanent magnets) can be arranged in series or in parallel, similar to the network in Fig. 6. [116]–[117] give an overview of nonlinear network solutions. Reference [3] gives a review of such magnetic circuits' terminal behavior and practical applications. Reference [92] shows how to derive the magnetic network from common parallel magnetization core geometries.

Orthogonal flux interaction requires the definition of magnetic quadripoles. In theory, mixed flux interaction may be split into (anti-)parallel and orthogonal flux interaction, though practical applications may require more specific models. Passive two-pole components' behavior to link flux and MMF is usually described as their reluctance  $R_m(\phi) = \frac{l}{\mu\phi}$  or differential reluctance  $R_{m,d}(\phi) = \frac{df}{d\phi}$  or their characteristic curve  $f(\phi)$ . These representations are generally equivalent, though for practical reasons, only the characteristic curve will be used in the following. A quadrupole can be regarded as two two-terminal networks whose states affect the other two-terminal network's characteristic.

Because there are other, more intuitive phenomena affecting a two-terminal network's reluctance, these are sometimes chosen to illustrate the effects of orthogonal magnetization. Assuming a homogeneous flux density, a region of the area  $A$ , the length  $l$  and the permeability  $\mu$  gives a reluctance  $R_m = \frac{l}{\mu A}$ . Therefore, a change in reluctance can be viewed as an according variation of geometry and permeability, e. g. in the VAG principle. However, the focus of this section was on literal description and no analogies. Any kind of (anti-)parallel fluxes can easily be represented within magnetic network models where several sources (e. g. coils or permanent magnets) can be arranged in series or in parallel, similar to the network in Fig. 6. [116]–[117] give an

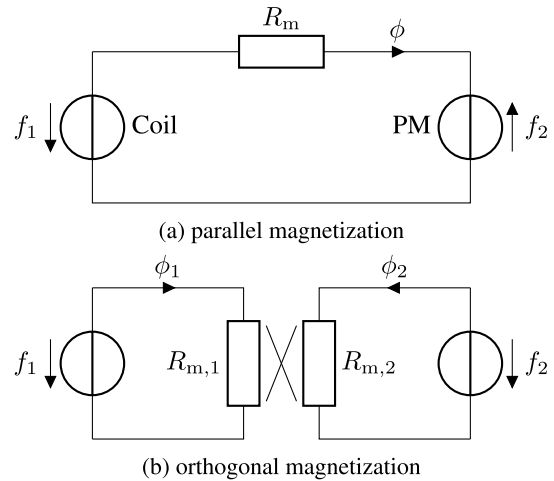


FIGURE 6. Magnetic networks with components representing ideal parallel and orthogonal magnetization. Parallel interaction follows (2), orthogonal one follows (6).

overview on nonlinear network solutions. Reference [3] gives a review of such magnetic circuits terminal behavior and practical applications. Reference [92] shows how to derive the magnetic network from common parallel magnetization core geometries.

### B. INTRINSIC INTERACTION

Two magnetic fields within the same RSI may not follow the principle of superposition but may react in a certain manner, as indicated above. The following shall investigate into appropriate representations of these interactions. It is worth noticing that fluxes shall be categorized into parallel and orthogonal. Other configurations must be split up into these components.

**Parallel flux** interaction follows two simple rules depending on whether the fluxes (parallel sources) or the MMFs (serial sources) add up

$$\begin{aligned} f(\phi_1, \phi_2) &= f(\phi_1 + \phi_2) \\ \phi(f_1, f_2) &= \phi(f_1 + f_2), \end{aligned} \quad (2)$$

where the material's magnetization curve  $h(b)$  respectively  $b(h)$  as well as the geometry ( $A$  and  $l$ ) ought to be known in order to define the component's characteristic curve:

$$f(\phi) = h\left(\frac{\phi}{A}\right) \cdot l \quad (3)$$

Antiparallel fluxes divert from this only with a change of sign, so their difference rather than their sum determines the material's point of operation. Still, there are a few assumptions to be made for (2) to apply:

- 1) Coupling between sources (coils, permanent magnets) and the core does not depend on total MMF or flux.
- 2) Coupling between sources and the core is equal for each source.
- 3) The fluxes are perfectly (anti-)parallel within the RSI.
- 4) Further flux interaction somewhere else (e. g. orthogonal) is represented separately.

Figure 6 includes two sources in series causing parallel flux interaction, one coil and one permanent magnet.

**Orthogonal interaction** requires a more complicated description. Figure 10a gives an idea of how orthogonal fluxes may be achieved. There are numerous assumptions made in the currently available models:

- 1) The magnetic material is isotropic, hence a scalar magnetization curve  $b(h)$  exists.
- 2) The magnetization curve is nonlinear.
- 3) The magnetization curve increases monotonically, therefore network solutions are distinct and the inverse magnetization curve  $h(b)$  exists as a function, too.
- 4) The magnetization curve goes through the origin.
- 5) The magnetization curve does not change under any influences, e. g. frequency.
- 6) The material causes no power losses (no eddy currents, no hysteresis loop).
- 7) The RSI contains a homogeneous material.
- 8) The RSI can be properly defined and described.
- 9) The magnetic fluxes are homogeneous within the RSI.
- 10) The RSI does not change under any influences, e. g. frequency, magnitude.
- 11) The magnetic fluxes are perfectly orthogonal within the RSI.
- 12) The resulting field's form is entirely independent from its magnitude.
- 13) The interacting fluxes do not interact anywhere else OR interaction elsewhere is modeled separately and compatibly.
- 14) There is no stray field.

However, following these assumptions, it becomes apparent that flux density over field strength can easily be calculated as

$$\begin{aligned} \mathbf{B}(H_1, H_2) &= \mathbf{B}(H_1\mathbf{e}_1 + H_2\mathbf{e}_2) \\ &= B(\sqrt{H_1^2 + H_2^2}) \cdot \frac{\mathbf{H}}{\sqrt{H_1^2 + H_2^2}}, \end{aligned} \quad (4)$$

where

$$\mathbf{B} = \begin{pmatrix} B_1 \\ B_2 \end{pmatrix}; \quad \mathbf{H} = \begin{pmatrix} H_1 \\ H_2 \end{pmatrix}; \quad \mathbf{e}_1 \perp \mathbf{e}_2 \quad (5)$$

and where the magnetization curve  $B(H)$  and its inverse function  $H(B)$  need to satisfy assumptions 1 – 7. Figure 7 illustrates the construction of the flux density  $\mathbf{B}$  from two given orthogonal field strengths  $H_1$  and  $H_2$  in comparison to the use of the inadequate superposition principle and Fig. 8 shows the difference of the results of the latter principle compared to the results of correct construction.

Equation 4 is equally valid to describe  $\mathbf{H}(B_1, B_2)$ . While the superposition principle assumes no interaction, the behavior described in (4) generates a double frequency flux density change as described in Fig. 9.

To derive the magnetic component's characteristic curves  $f_1(\phi_1, \phi_2)$  and  $f_2(\phi_1, \phi_2)$  for the non-trivial case that the

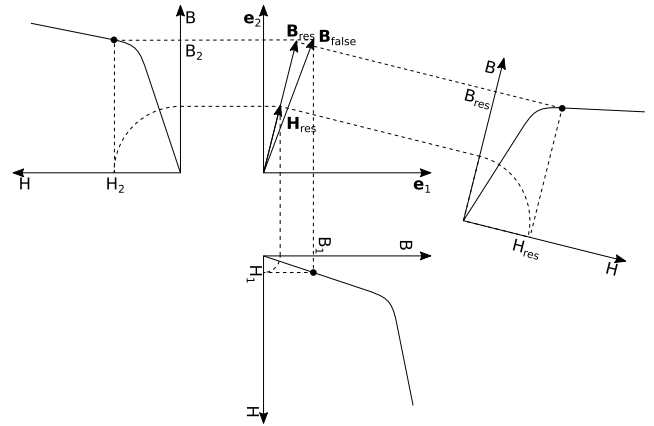


**FIGURE 7. Two given orthogonal field strengths  $H_1$  and  $H_2$  with larger and falsely oriented resulting flux, assuming no interaction  $B_{\text{false}} = B(H_1)\mathbf{e}_1 + B(H_2)\mathbf{e}_2$  than actually resulting flux  $B_{\text{res}}$  according to (4) [92].**

orthogonal field is non-zero, the RSI's geometry must be taken into account. The concerning assumptions 10 – 13 can only be achieved with a torus-shaped core (see Fig. 10b), though an analytical solution may be impracticably complex according to [92] and numerical approximations of sorts may be required. Assumptions 8 – 9 can be achieved by a very thin torus, whose effective areas and lengths can be defined as  $A_1, l_1, A_2$  and  $l_2$ .

The characteristic function

$$f_k(\phi_1, \phi_2) = \frac{l_k}{A_k} \phi_k \cdot \frac{h\left(\sqrt{\frac{\phi_1^2}{A_1^2} + \frac{\phi_2^2}{A_2^2}}\right)}{\sqrt{\frac{\phi_1^2}{A_1^2} + \frac{\phi_2^2}{A_2^2}}} \quad \forall k \in \{1; 2\} \quad (6)$$

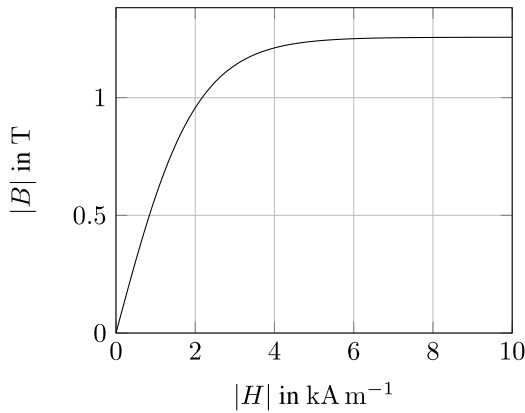
then describes the magnetic component perfectly [92]. Of course, the above definitions of reluctance and differential reluctance are applicable to this relation.

Finally, assumption 14 ensures that the magnetic fluxes actually flow through the regarded RSI which is generally true for a proper core design. However, at points of operation far into the material's saturation, this becomes less applicable.

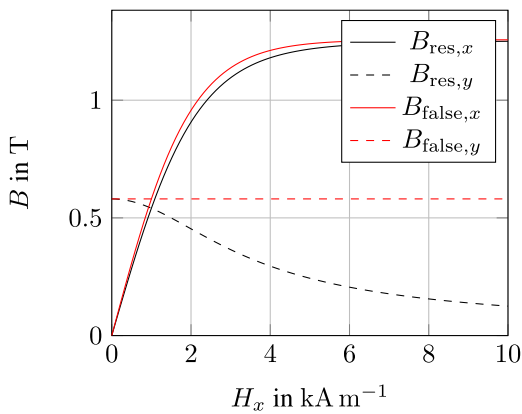
**Deviations from the ideal theory** appear in real setups. Despite a decent application design, the following errors may appear and void the above theory:

- 1) The core material is nonisotropic, causes losses and depends on frequency and possibly other influences.
- 2) Mixed interaction may be difficult to properly split up analytically.
- 3) Most orthogonal interaction cores show parallel magnetization somewhere else in the core [92].
- 4) Often no separate paths for both orthogonal fluxes, therefore interaction in different regions and no perfect orthogonality [92].
- 5) Flux densities are not homogeneous.
- 6) Field's form depends on flux magnitude.
- 7) RSI depends on flux magnitude.
- 8) Generally no properly definable RSI.

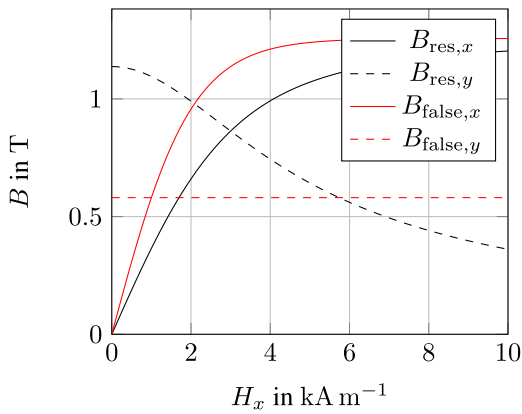




(a) characteristic curve



(b)  $H_y = 1 \text{ kA m}^{-1}$



(c)  $H_y = 3 \text{ kA m}^{-1}$

**FIGURE 8.** Resulting fluxes assuming no interaction  $B_{\text{false}} = B(H_1)e_1 + B(H_2)e_2$  and actually resulting flux  $B_{\text{res}}$  according to (4).

All material properties mentioned under deviation 1 invalidate the above intrinsic orthogonal interaction model. There is currently no fundamental theory on the quantitative behavior of real orthogonal or mixed magnetization applications.

There is currently no approach on how to separate mixed magnetization into parallel and orthogonal, so further theory is needed before applying the above models for intrinsic

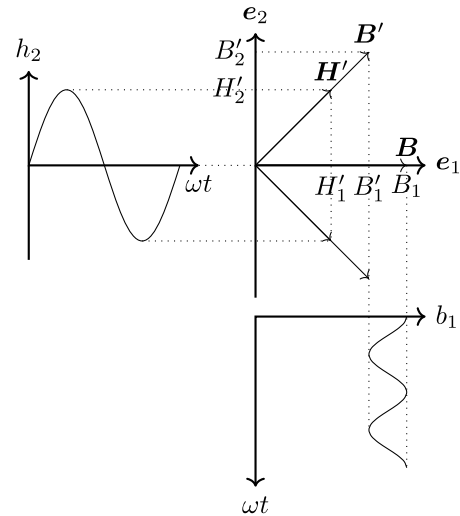


**FIGURE 9.** General principle of orthogonal flux interaction where a varying  $h_2$  influences  $b_1$  despite constant  $h_1$ .  $B$  at  $h_2 = 0$  and  $B'$  at maximum  $h_2$ . The resulting primary flux densities wave form  $b_1(\omega t)$  shows even harmonics and depends on form and magnitude of the secondary field strength  $h_2(\omega t)$ , the magnetization curve's  $b(h)$  exact form and also geometry ( $A$  and  $l$ ) [92].

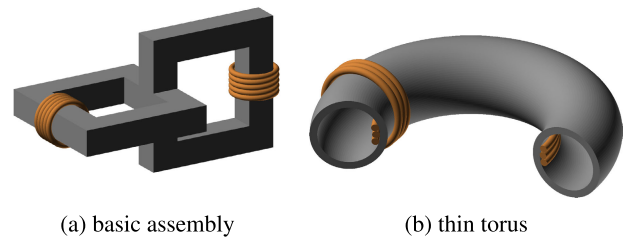


**FIGURE 10.** Examples of magnetic cores implementing orthogonal magnetization [92].

interaction. The difficulty arises from the very inhomogeneous and magnitude-dependent distribution of the field's direction vectors due to the non-linear material, so that the magnetic field's form (directions and relative magnitudes) are extremely difficult to calculate with conventional methods. However, [118] shows clearly, that numerical calculation (FDM, FEM) can serve properly to apply the intrinsic interaction model to any geometry.

As already mentioned in [92], applications relying on orthogonal flux interaction must not have parallel flux in any regions within the core. At the same time, geometries as in Fig. 10 are difficult to manufacture and may be resource-intensive.

Fig. 21 and Fig. 22 demonstrate that deviations 5 – 8 occur even before applying an orthogonal flux, especially at operating points deep into saturation.

### C. ELECTRIC TERMINAL BEHAVIOR

Given the interaction between two fluxes (split up into an (anti-)parallel and an orthogonal part) by (2) and (6), the terminal behavior of typical magnetic applications can be derived by applying the above relations between magnetic and electric network entities.

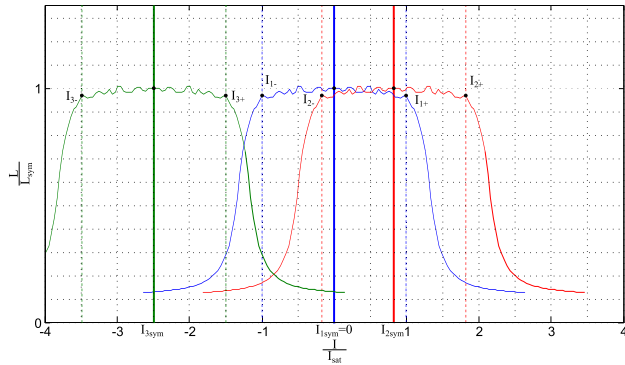


**FIGURE 11. Quantitative example for electric terminal behavior of a parallelly influenced inductance.  $L(I)$  curve shifted along  $I$  axis with permanent magnets [3].**

It is important to notice, that other than electric networks, whose change in state merely result in a change of the current power flow, magnetic networks' changes of state result in a change of energy distribution due to the time-integral nature of the magnetic flux  $\Phi = \frac{1}{N} \int u dt$ . Therefore, all flux interaction can be used to transport energy, possibly between two current-carrying coils. This principle is used in transformers which are based parallel magnetization and in paraformers, based on orthogonal flux interaction. There is precise analytical theory available to determine the stability and point of operation of electric networks involving an orthogonal interaction magnetic circuit and at least one capacitor. Reference [92] gives an overview over the applied Mathieu and Hill equations for real paraformers, which shall not be discussed in this article any further.

Parallel and anti-parallel magnetization with a permanent magnet providing a constant MMF  $f_{pre}$  simply shifts the  $L(I)$  curve along the  $I$ -axis about  $\frac{1}{N}f_{pre}$ . Both terms add up for parallel fluxes and subtract for anti-parallel ones:

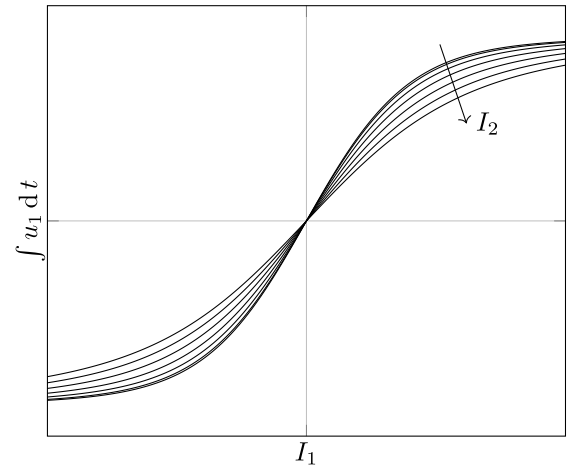
$$L(I, f_{pre}) = L\left(I \pm \frac{1}{N}f_{pre}\right) \quad (7)$$

Fig. 11 illustrates the result. It should be mentioned, that a nonlinear parallel magnetic source will distort the  $L(I)$  curve.

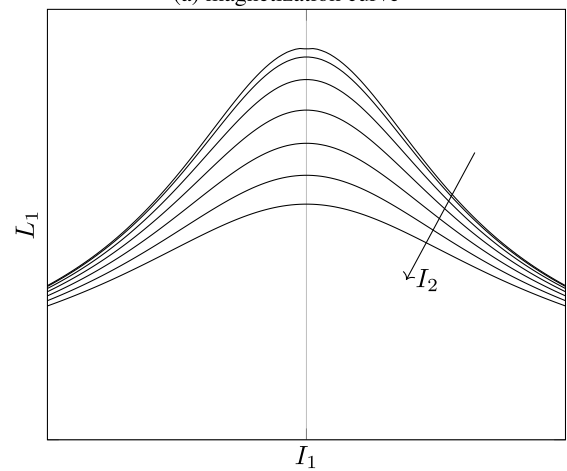
Orthogonal flux interaction has already been investigated above and the magnetic network entities in (6) can be converted into the electric terminal entities as already mentioned before. However, this conversion results in a more complicated behavior than with parallel magnetization. Fig. 12 shows an example of an orthogonal interaction magnetization curve and the according  $L(I)$  curve with  $L := \frac{1}{I} \int u dt$ .

#### D. SUMMARY

It could be shown that, with the help of various suitable assumptions, a calculation of flux interactions is analytically possible. The investigations were related to the current view of magnetic circuits using selected literature. They thus provide the basis for understanding simulations and measurements and help to interpret these results accordingly. Of particular importance in the chosen approach are the extensive assumptions. In future investigations, the listed assumptions



(a) magnetization curve



(b) Inductance

**FIGURE 12. Qualitative example for electric terminal behavior of an orthogonally influenced inductance according to (6).**

should be analysed in detail to further detail the analytical modelling.

## IV. SIMULATION RESULTS

To get a deeper understanding of the processes within the magnetic core during a flux interaction of differently aligned magnetic fields, 2D and 3D simulation are a suitable methods to illustrate, e.g., the saturation level of the different core areas. The following section provides an overview of various simulation results of the different biasing methods introduced in Sec. II using the software FEMM and Ansys Maxwell.

The simulations were carried out for different core materials because the manufacturer could only provide these special combinations of machined core materials and core geometries.

### A. PARALLEL BIASING

To show the impact of parallel biasing, a magnetic amplifier is simulated using FEMM. The main winding is located on the center leg and is wound counterclockwise, whereas the two

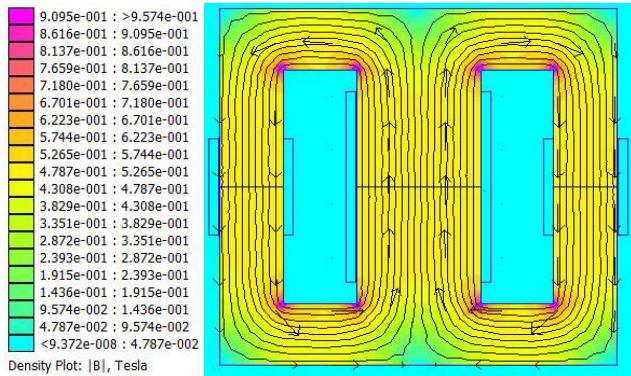


FIGURE 13. Simulation results of a magnetic amplifier with  $I_{aux} = 0$  A.

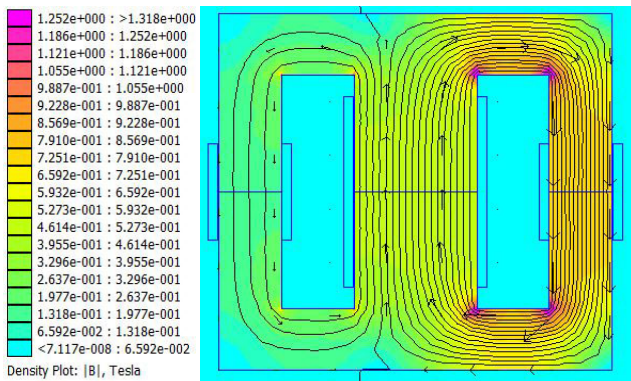


FIGURE 14. Simulation results of a magnetic amplifier with  $I_{aux} = 1$  A.

auxiliary windings are located on the two outer legs. The left winding is also wound counterclockwise, the right winding is wound clockwise. For simulation, an E70/33/32 core made of “N87 material” (EPCOS/TDK) is used.

In Fig. 13, the auxiliary bias current is  $I_{aux} = 0$  A. The main magnetic flux is evenly distributed to the two outer legs. The saturation of the core is at a medium level. The auxiliary bias current is increased to  $I_{aux} = 1$  A in Fig. 14. The auxiliary magnetic flux within the left leg is oppositely aligned to the main magnetic flux, while the auxiliary magnetic flux within the right leg is aligned in the same direction. The overall magnetic flux and its density within the left leg decrease, while they increase within the right leg.

If the direction of the auxiliary bias current changes, the left leg will show a higher flux density, whereas the right leg will be stressed to a lesser extent. The resulting auxiliary current will affect all outer legs as well as the yokes, only the center leg will remain unaffected.

**B. MIXED BIASING**

According to section II an application of mixed biasing is a VAG-VR. Figures 15 – 17 show a VAG-VR that was used for verification measurements in [119]. It is an E34/14/9 core made of “3C90 material” (Ferroxcube), which is simulated using Ansys Maxwell. The air gap is 1 mm. To introduce the auxiliary bias winding into the core, four holes with a

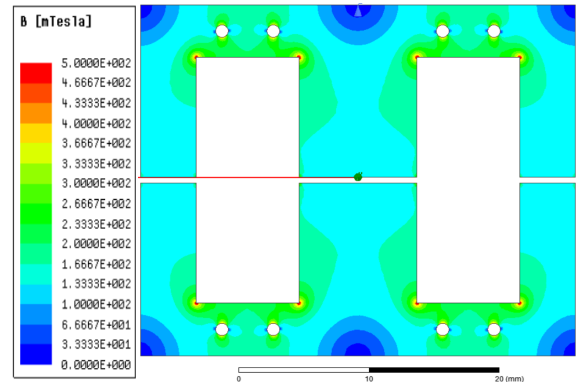


FIGURE 15. Simulation results of a mixed biased ferrite E-core with  $I_{aux} = 0$  A [119].

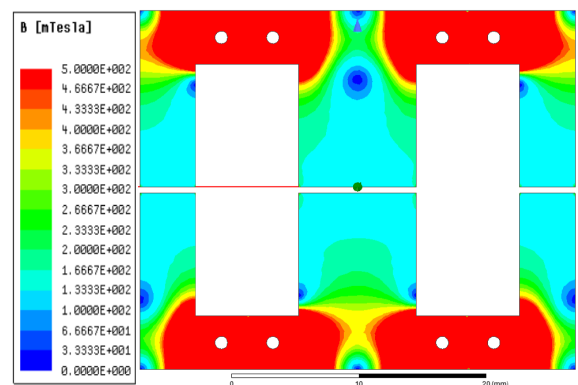


FIGURE 16. Simulation results of a mixed biased ferrite E-core with  $I_{aux} = 20$  A [119].

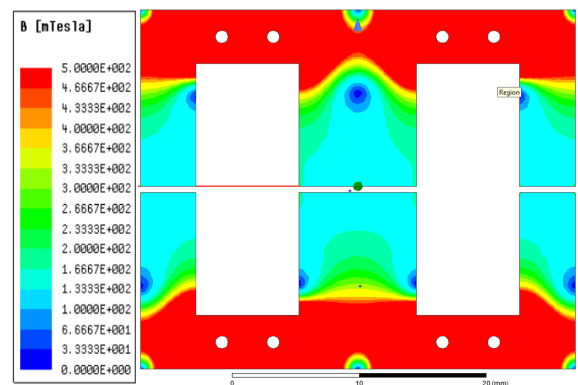
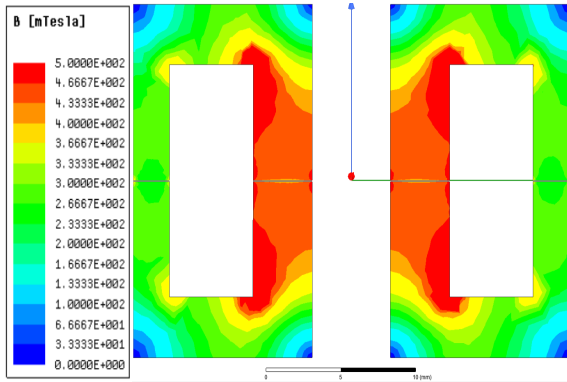


FIGURE 17. Simulation results of a mixed biased ferrite E-core with  $I_{aux} = 40$  A [119].

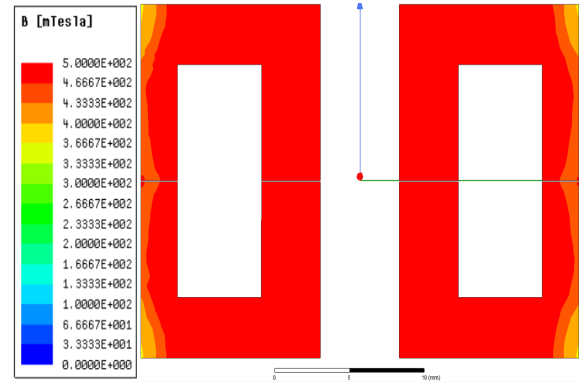
diameter of 1 cm are drilled in both the upper and lower yoke. The auxiliary bias current is increased from  $I_{aux} = 0$  A up to  $I_{aux} = 40$  A.

Figure 15 shows the simulation results of the core’s flux density for  $I_{aux} = 0$  A. The flux density is still low in the yokes as well as in the center leg and the outer legs.

By increasing the auxiliary current to  $I_{aux} = 20$  A (Fig. 16), simulation results show a significant saturation in the upper and lower yoke within the area around the drill holes. The



**FIGURE 18.** Simulation results of a orthogonal biased ferrite P-core with  $I_{aux} = 0$  A [119].



**FIGURE 20.** Simulation results of a orthogonal biased ferrite P-core with  $I_{aux} = 40$  A [119].

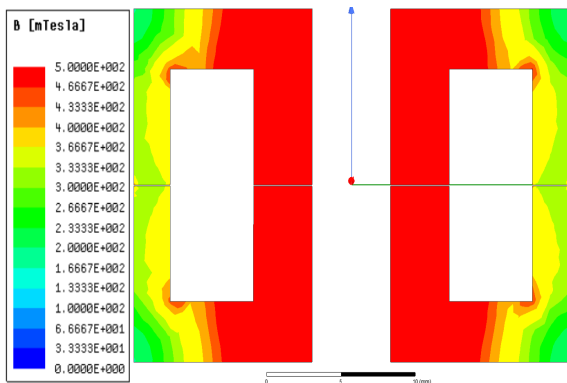


**FIGURE 19.** Simulation results of a orthogonal biased ferrite P-core with  $I_{aux} = 20$  A [119].

center leg and the outer legs are unaffected. The saturation does not change, especially close to the air gap.

At an auxiliary current of  $I_{aux} = 40$  A (Fig. 17), the saturation spreads within the yoke and affects the passages to the legs. The middle section of the legs is still unaffected.

The permeability of the saturated core material decreases significantly. The whole saturated area behaves like an air gap, what leads to an adjustable and controllable reluctance of the magnetic core. If the drill holes are introduced into the center leg or the outer leg, these sections will saturate while the yokes and the unmachined leg/s are unaffected.

### C. ORTHOGONAL BIASING

If the core material is isotropic, the VAG concept can be used as orthogonal biasing. The core in Fig. 18–20 is also used for verification measurements in [119]. It is an P30/19 core made of “3C90 material” (Ferroxcube), which is simulated using Ansys Maxwell. The air gap is 0.14 mm. The P core already has a hole within the center leg, so drilling is not necessary. As well as the investigations regarding mixed biasing, the auxiliary bias current is increased from  $I_{aux} = 0$  A up to  $I_{aux} = 40$  A.

If no auxiliary current flows ( $I_{aux} = 0$  A), the middle section of the center leg shows a high flux density whereas the flux density, in the outer ring leg is low (Fig. 18).

By increasing the auxiliary current to  $I_{aux} = 20$  A (Fig. 16), simulation results show a significant saturation in the center leg. Even the outer ring leg is affected.

In Fig. 17, the auxiliary current is increased up to  $I_{aux} = 40$  A. The saturation spreads from the center leg to the outer ring until almost the whole core is saturated.

If the whole core saturates, the magnetic device’s behavior is close to an air coil. The inductance value is at its minimum and cannot decrease anymore.

### D. LACKING HOMOGENEITY

Fig. 21 proposes a possible section of a magnetic core intended to show orthogonal flux interaction between some vertically and horizontally oriented flux. While Fig. 21a shows the vertical flux’s distribution within the RSI and the surrounding area (vertical arms and air), Fig. 21b demonstrates how the horizontal arms affect the vertical flux, even with absolutely no source on the horizontal circuit. It should be mentioned that Fig. 21 shows a point of operation deep into the material’s saturation. More than half of the flux escapes the intended RSI.

It might appear intuitive to try and prevent this phenomenon by using isotropic materials or isotropic geometry. Figure 22 demonstrates the use of longitudinal air gaps (LAGs) in the cross’s arms, where they are in parallel to the wanted and orthogonal to the unwanted flux. Of course, they end right before the RSI. Unfortunately, this measure makes only little difference with regards to properly defined flux distribution. Instead, flux now escapes the RSI deep in the horizontal arms causing parallel, antiparallel, mixed and orthogonal magnetization outside the RSI in a poorly predictable and describable way.

Despite the abovementioned ineffective attempts to obtain homogeneous flux density, there is a promising core geometry: By bending a flat and rectangular piece of magnetic core into a pipe, the tangential flux never leaves the RSI because there is no further magnetic circuit required. If the pipe is bent into a thin, hollow torus (see Fig. 10b), both flux distributions are perfectly perpendicular towards each other in each point within the torus and no further magnetic material

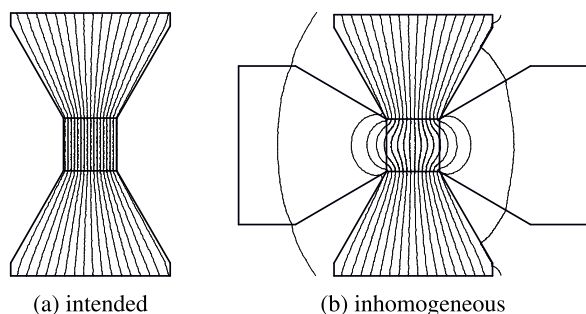


**FIGURE 21. Saturated cross for orthogonal flux interaction. M-15 steel in air. Flux between top and bottom arm saturating region in space of interaction (middle square). Left and right arms carrying only unintentional flux. 10 flux lines escaping into left and right arms, 6 flux lines within region but not properly oriented, 2 flux lines as intended.**

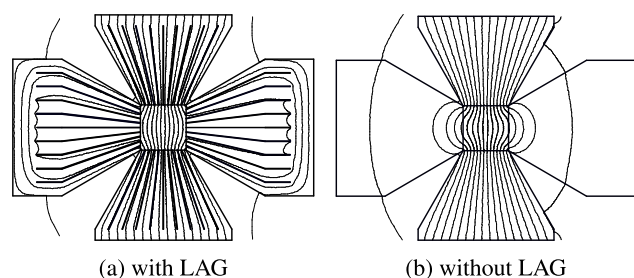


**FIGURE 22. Saturated cross for orthogonal flux interaction with LAGs. M-15 steel in air. Flux between top and bottom arm saturating region in space of interaction (middle square). Left and right arms carrying only unintentional flux. LAGs distort the field even further. 8 flux lines escaping into left and right arms, 6 flux lines within region but not properly oriented, 4 flux lines as intended.**

is needed. However, even though such a geometry has already been proposed in [92], it appears to not have been built ever since.

**E. DISCUSSION OF SIMULATIONS**

Simulation results are a significant help in research and development. They enable a deeper understanding of the physical processes within the core material and support the design and evaluation process.

However, it should be considered that the simulations' accuracy is highly dependent on the used parameters and boundary conditions. The simulation results can just be as reliable as the mathematical model behind the software.

Most simulation software programs are very precise for specific applications. In divergent cases, they might be unsuitable. Furthermore, the data input is very important to achieve a high precision. Many simulation software programs are able to read hole hysteresis data of the used material. This is highly recommended to achieve a high accuracy.

For the executed simulations in Ansys Maxwell and FEMM magnetization curves based on the data sheets of the ferrites were used. The boundary conditions were set to default as recommended by the software manufacturers. In Ansys Maxwell, the mesh conditions were increased compared to the suggested settings to avoid further iterations and

due to sufficient simulation time. A verification was done regarding the sufficient meshing and boundary conditions for the modeling.

**F. SUMMARY**

The simulation results have shown how the three flux interaction methods affects the core material. While parallel biasing usually affects the whole core, mixed biasing just affect an area around the drill holes. Other sections of the magnetic core, which are further away, stay unaffected. If orthogonal biasing is used, the saturation spreads from the center to the outside and is able to affect the whole core geometry.

Furthermore, it has to be said, that suitable and precise simulation conditions are essential to get accurate simulation results.

A cross-shaped structure was introduced for further investigations and adjustments of this structure were also discussed. This structure will be used, similar to a single sheet tester, in future investigations, especially to be able to adjust and improve the analytical model with simplified simulated results and measurements.

**V. MEASUREMENT RESULTS**

In this section, measurement results for the different methods of field superposition based on different setups are presented and explained. The focus is on E cores, because all variants can be realized very well with these cores. Small-signal measurements with impedance meters and large-signal measurements for evaluation of the hysteresis and magnetization curves are performed. For the small-signal measurements, the Precision Magnetics Analyzer 3260B from Wayne Kerr and the Impedance Analyzer Bode 100 from Omicron Lab are used. A sine voltage of small amplitude is applied to the DUT by the measuring device and the subsequent current and phase shift are measured. This allows the impedance calculation of the DUT and, based on this, further characteristics such as a series inductance and a series resistance. The measurement is carried out at a sine wave voltage with  $U_{rms} = 1\text{ V}$  and any frequency (frequency sweep). For large-signal measurements, a fixed frequency is selected, while the voltage can be adjusted variably. Different voltages allow variable control of the component, which is crucial due to the nonlinear effects. The size of the flux linkage  $\Psi$  can be measured via an integrating low-pass filter. By additionally measuring the current, a hysteresis curve ( $\Psi(I)$ -curve) can be generated on the oscilloscope. A frequency of 250 Hz is selected for these measurements. This frequency is not in the high-frequency range, although this is the application range of ferrites. The reason is, that due to the relatively large inductance of about 3 mH, a very large voltage would be required to drive the core or even parts of it into saturation.

As with the simulations, the measurements were carried out for different core materials because the manufacturer could only provide these special combinations of machined core materials and core geometries.

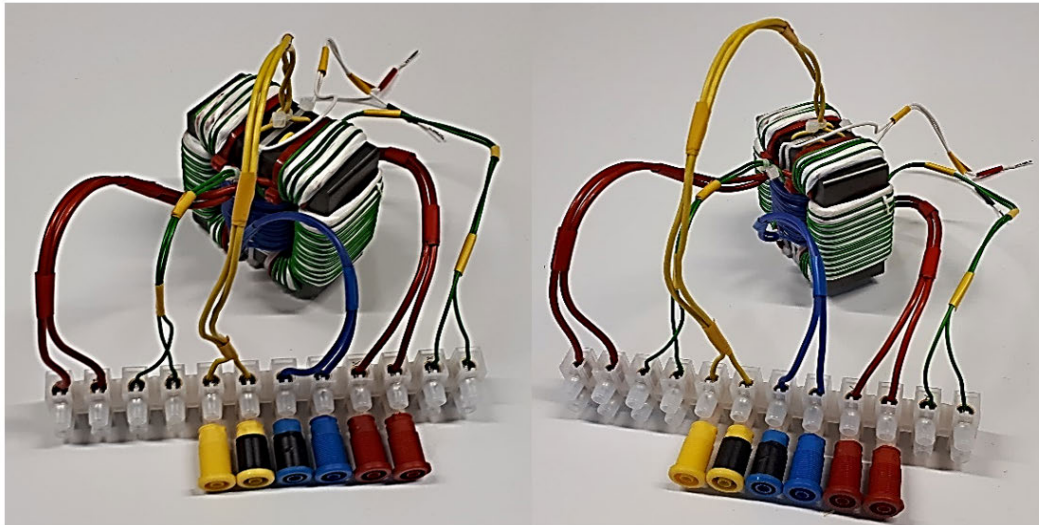


FIGURE 23. DUT for parallel biasing.

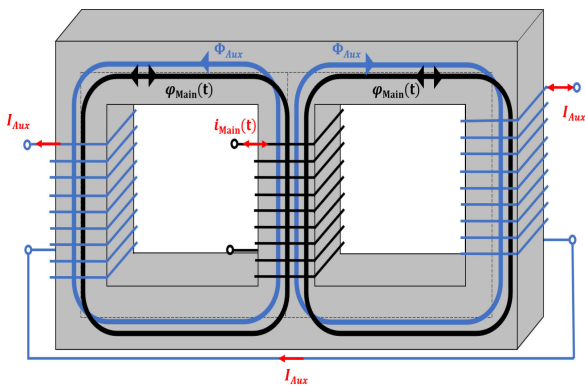


FIGURE 24. Winding connection at the DUT for parallel biasing (Test 1).

A. PARALLEL BIASING

The parallel bias appears quite trivial, but large-signal measurements produce very unusual hysteresis curves. An MnZn E core (E70/33/32) is used for the measurements (see Fig. 23). This core has windings on the middle leg (blue winding) and outer legs (red windings). The yellow winding is not interesting for parallel premagnetization and the green and white windings are used for measuring.

For a first measurement, an alternating current is impressed on the winding of the middle leg and the measurement is carried out on a second winding on this leg. The auxiliary current  $I_{Aux}$  is impressed on the windings of the outer leg (see Fig. 24). The generated DC magnetic field in the middle leg, is either in the opposite or in the same direction as the alternating field, depending on the sign of the alternating current.

The DC magnetic field creates a new operating point on the magnetization characteristic line. If this operating point is placed close to the saturation range, strong deformations of the hysteresis curve occur (see Fig. 25). Since the

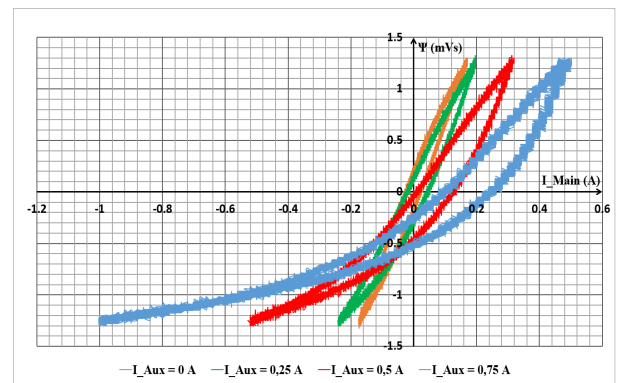


FIGURE 25. Hysteresis-curves at parallel biasing (Test 1).

measurement was made with a low-pass filter, the shift into the operating point is not visible. Only the deformation of the hysteresis curve can be reproduced. Furthermore, the hysteresis curve is not fully modulated to avoid high saturation currents when the operating point is shifted. The peak-to-peak value of the input voltage was not changed during the measurements.

As the auxiliary current increases, the operating point is moved further and further into the saturation range. A significant change in inductance becomes visible. However, it should be emphasized that all commutation points lie on the same commutation characteristic curve. With this type of premagnetization, therefore, the nonlinear properties of the magnetization characteristic curve are exploited to a large extent. A completely different behavior can be observed with parallel premagnetization due to a modified wiring of the windings on the outer leg and the measurement of the hysteresis curve on the outer legs. The auxiliary current for premagnetization is now fed into the winding on the middle leg. The alternating current is accordingly generated by the windings on the outer leg.

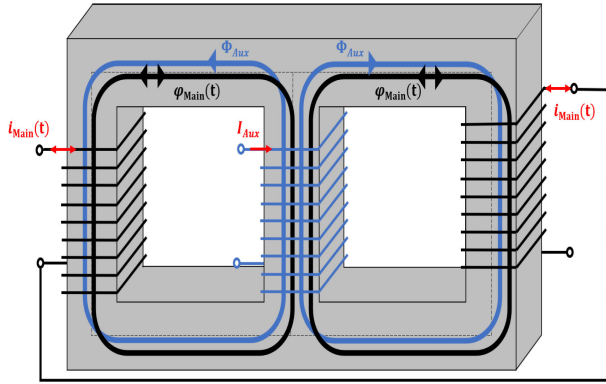


FIGURE 26. Winding connection at the DUT for parallel biasing (Test 2).

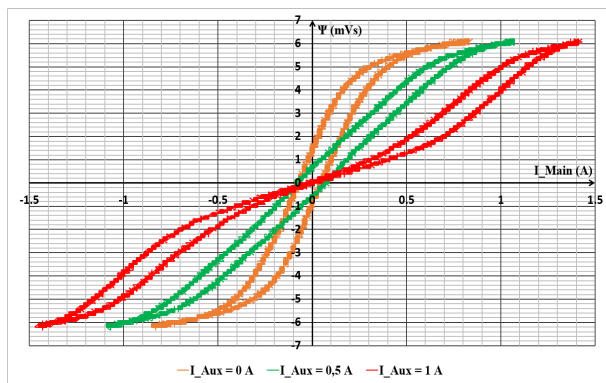


FIGURE 27. Hysteresis-curves at parallel biasing (Test 2).

Due to the wiring shown in Fig. 26, the alternating flow in the middle leg of the core is cancelled. The connection of the measuring winding on the outer leg is done in the same way. The bias flux generated by the auxiliary current is in one outer leg in the same direction as the alternating flux, while the alternating flux is in the opposite direction in the second outer leg.

Due to the special circuitry, the hysteresis curve is deformed at high auxiliary currents in such a way that a double S curve is created (see Fig. 27).

**B. MIXED BIASING**

In the following, the measurement results of the mixed premagnetization are presented and explained. The same E core (E70/33/32) (see Fig. 28) is used as in the measurements for mixed premagnetization. In this core, twelve holes are drilled horizontally through the middle leg. A wire (yellow) is passed through the holes in such a way that directly adjacent wires carry the direct current  $I_{aux}$  in opposite direction.

The measurements are carried out on the white winding on the middle leg. In addition, a direct current can feed into on the blue winding on the middle leg in order to set an operating point on the magnetization characteristic curve.

The result of the mixed premagnetization is again a double S curve with a kind of Rayleigh loop around the zero point as it is shown in Fig. 29. For an auxiliary current  $I_{aux} = 2 A$ ,

the hysteresis curve is deformed rather than resembling a double S curve. Only for currents that increase in magnitude, the described shape becomes clearly visible. The effect can easier be seen by calculating the magnetization curves (see Fig. 30). To describe the behavior, the following simple transformer with UI core is considered (see Fig. 31) [120]. The part in the winding window of the transformer is designed as a controllable unit [120].

The tangent hyperbolic function can be used to approximate the magnetization characteristic of a magnetic section. For the structure that ensues, the following relationship results for the magnetization characteristic curve of the controllable unit in the center of the core:

$$\Phi_1(F_1) = B_{sat} \cdot A_{eff} \cdot \left( \tanh\left(\frac{\mu_0 \cdot \mu_r \cdot (F_1 + N \cdot I_{aux})}{B_{sat} \cdot l_{eff}}\right) + \tanh\left(\frac{\mu_0 \cdot \mu_r \cdot (F_1 - N \cdot I_{aux})}{B_{sat} \cdot l_{eff}}\right) \right) \quad (8)$$

$A_{eff}$  is the area of the center UI core in Fig. 31.  $l_{eff}$  is the length from the middle of the center UI core’s upper yoke to its lower yoke. The result is shown in Fig. 32. It is again a double S curve, for an increase in direct currents  $I_{aux}$  and for a fictitious core.

If only two adjacent holes of the original structure (as shown in Fig. 33) are considered, a similar relationship to Fig. 31 can be identified.

The main flow is on the two outer sides of the leg, in the opposite direction to the flow generated by the auxiliary current, and in the middle, it is in the same direction. In addition, the area in the middle is approximately twice as large as the area on the outside of the leg. However, problems in the calculation are caused by those parts that are not parallel or antiparallel to the main flow. This is one of the main reasons why the measured characteristic curve differs from the theoretical characteristic curve of the simple replica, but also from the previously measured characteristic curve with a purely parallel premagnetization. In Fig. 34 and Fig. 35, the small-signal measurements for the core are now shown. The percentage change of the series inductance at a set current  $I_{aux}$ ,  $y$  is given, in each case related to the inductance at the frequency  $f_z$  and a current  $I_{aux} = 0 A$ . In addition, the set current in the main winding  $I_1$ ,  $x$  must be considered.

$$\Delta L = \frac{L(I_1, I_{aux}, f_z) - L(I_1, I_{aux} = 0, f_z)}{L(I_1, I_{aux} = 0, f_z)} \quad (9)$$

The main current  $I_1$  adjusts the operating point on the magnetization curve during the small-signal measurement and the current  $I_{aux}$  changes the shape of the hysteresis curve, as shown by the large-signal measurement. The dependence on the frequency is caused by the permeability on the one hand and by parasitic effects of the test setup as well as the test object on the other hand.

By increasing the current  $I_{aux}$ , the inductance can be significantly reduced. The reason is that the magnetization characteristics at the zero point  $I_1 = 0 A$  are sheared significantly

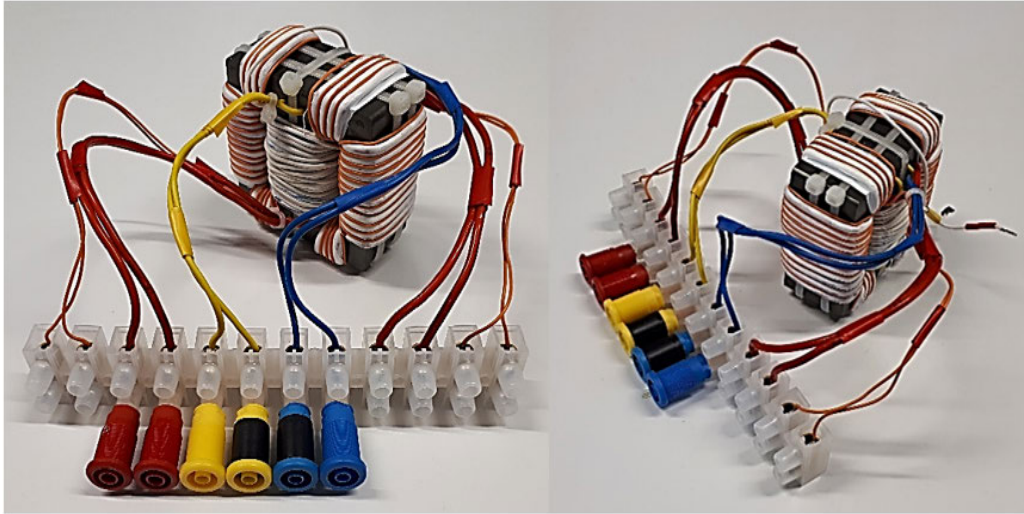


FIGURE 28. DUT for mixed biasing.

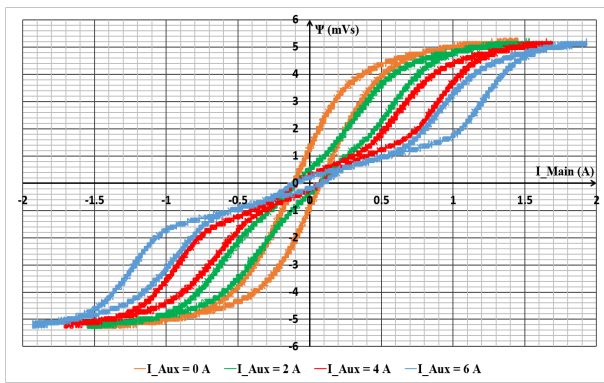


FIGURE 29. Hysteresis curves at mixed biasing.

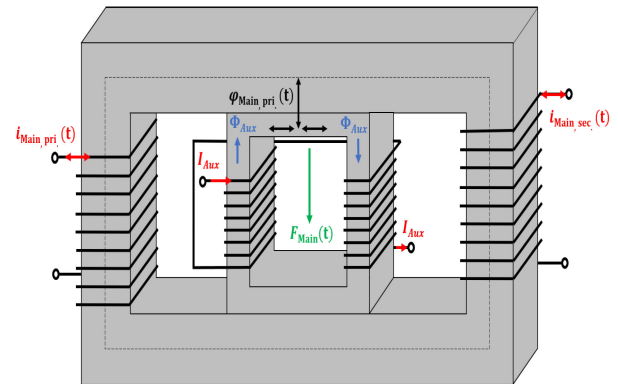


FIGURE 31. Controllable transformer for comparison to mixed biasing.

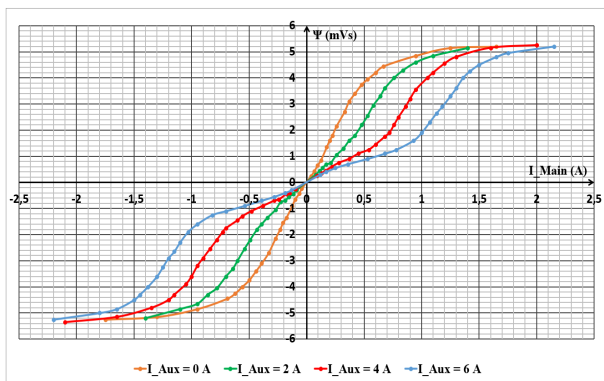


FIGURE 30. Magnetisation curves at mixed biasing.

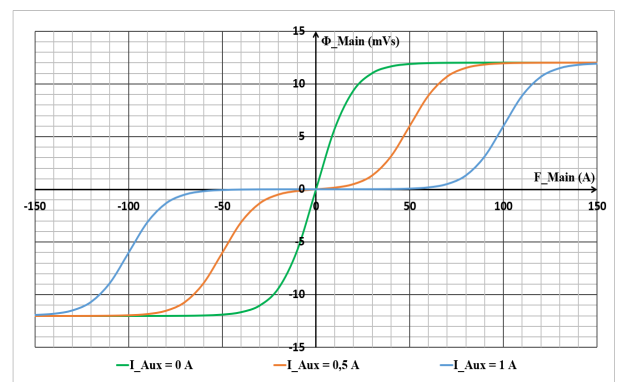


FIGURE 32. Calculated magnetization curves for the controllable part of the transformer according to Fig. 31. Taken and adapted from [120] with  $B_{sat} = 1.2 T$ ,  $\mu_r = 25\,000$ ,  $I_{eff} = 0.5 m$ ,  $A_{eff} = 50 cm^2$  and  $N = 100$ .

and therefore have a much smaller slope. This can be change depending on the operation point. With a main current  $I_1 = 1 A$ , the opposite behavior is present.

This behavior can be explained by the fact that the current  $I_{aux}$  generates a new magnetization characteristic

(see Fig. 30). If we now compare the characteristics at a main current  $I_1 = 1 A$ , we can see that the core is already saturated at this operating point and a current of  $I_{aux} = 0 A$ . However, for increasing auxiliary currents, the slopes of the respective



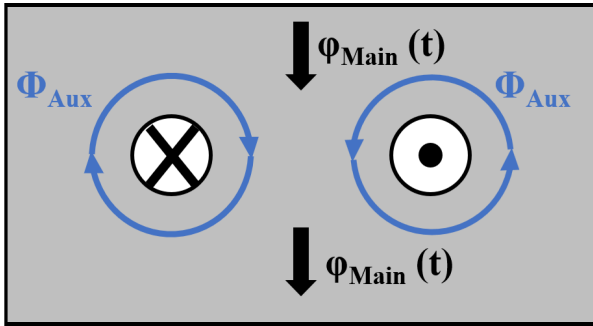


FIGURE 33. Schematic structure for mixed biasing.

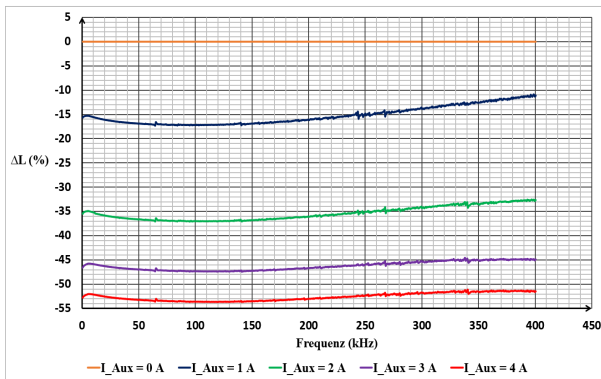


FIGURE 34. Measurement results of small-signal measurements at mixed biasing and  $I_1 = 0$  A.

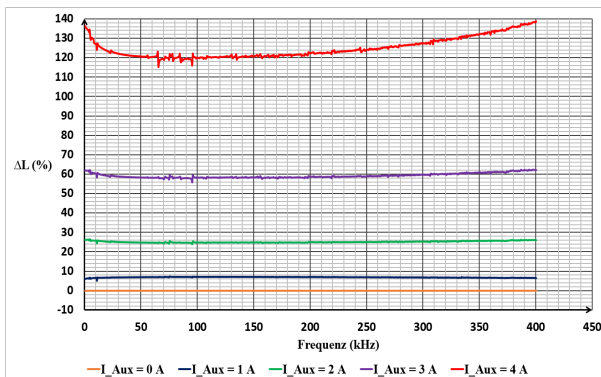


FIGURE 35. Measurement results of small-signal measurements at mixed biasing and  $I_1 = 1$  A.

magnetization characteristics become larger at this operating point. It should be noted that the increase of about 120% to 135% refers to the inductance at  $I_{aux} = 0$  A at the same operating point and not to the originally designed inductance in the linear range. Accordingly, a 3D diagram, as it is shown in Fig. 36, can be displayed for a selected frequency showing the inductance as a function of the main current  $I_1$  and the auxiliary current  $I_{aux}$ .

Of particular interest in Fig. 36 is the range of high auxiliary currents and main currents in the 500 mA range. In this range a local maximum of inductance can be seen. This can be explained by the fact that with low main currents and high

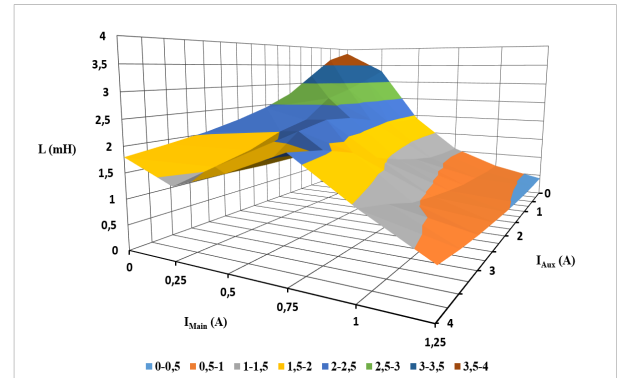


FIGURE 36. Inductance depending on  $I_1$  and  $I_{aux}$  at mixed biasing ( $f = 100$  kHz).

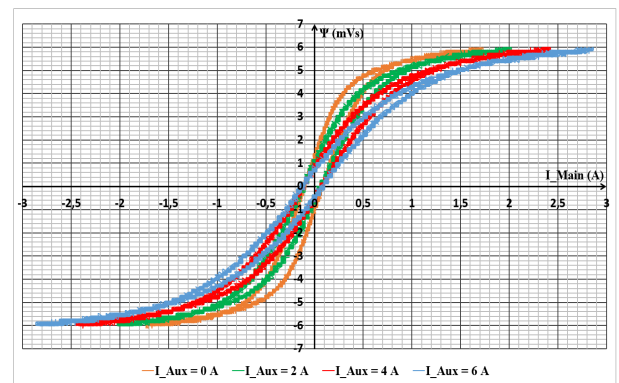


FIGURE 37. Hysteresis curves at orthogonal biasing.

auxiliary currents, the magnetization characteristic curve initially runs in a very flat manner due to the double S shape. As the main currents increase, however, the operating point is shifted to steeper sections of the curve, which is noticeable by a larger inductance.

### C. ORTHOGONAL BIASING

For the investigations of the orthogonal premagnetization, the E core according to Fig. 23 is used, whereby in this case six holes are drilled vertically into the center leg of the core. Like the experiments for mixed bias magnetization, lines directly adjacent to each other carry opposite currents. Also, in this DUT, the currents are marked  $I_{aux}$  by the yellow windings and the measurements are carried out on the white winding on the middle leg, whereby the blue winding on this leg can be used to set the operating point.

The measurement results of the orthogonal premagnetization (see Fig. 37 and Fig. 38) show that the original hysteresis curve at  $I_{aux} = 0$  A is sheared. For increasing auxiliary currents, the curve becomes flatter, which is equivalent to a decreasing inductance. In the equivalent circuit diagram, this in turn means an increasing magnetic resistance. This behavior is easy to understand, as the equivalent circuit diagram can be expressed by a series connection of two resistors. The total

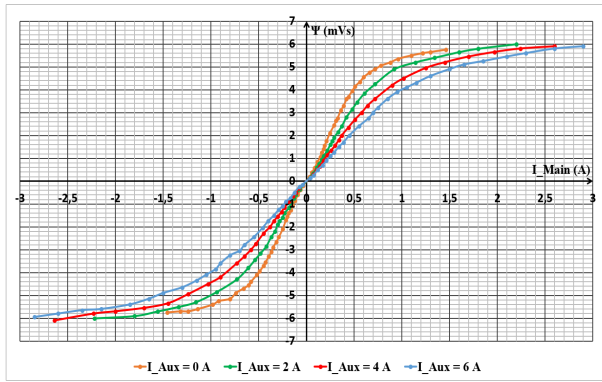


FIGURE 38. Magnetisation curves at orthogonal biasing.

resistance results from the sum of the parallel connection of the two resistors of the outer leg ( $R_{mag, \text{outer-leg}}$ ) and the resistance of the center leg ( $R_{mag, \text{center-leg}}$ ).

$$R_{mag, total} = \frac{N^2}{L} = \frac{R_{m, \text{outer-leg}}}{2} + R_{m, \text{center-leg}} \quad (10)$$

While the permeability of the middle and outer leg is changed equally by the main current  $I_1$ , the permeability of the middle leg is additionally influenced by the auxiliary current  $I_{aux}$ . For an increasing auxiliary current, the permeability of the middle leg decreases, which increases the resistance. In sum, this leads to an overall increase in resistance, which in turn results in a decrease in inductance. In the following, the small-signal measurements are shown in Fig. 39 and Fig. 40. The same representation is chosen as for the subsections before.

If the main current  $I_1 = 0$  A, the inductance decreases as expected for increasing auxiliary currents. The reason for this is that there is a smaller gradient in the  $\Psi(I)$  characteristic due to the sheared magnetization characteristic.

If the main current  $I_1 = 1$  A, an additional current  $I_{aux}$  does not reduce the inductance but can even increase it by 50%. This can be explained by the fact that current  $I_{aux}$  gives the component a new magnetization characteristic. Thus, with a main current of  $I_1 = 1$  A and a current  $I_{aux} = 0$  A, the core is at the beginning of saturation, which means a very flat magnetization characteristic. At a current of  $I_{aux} = 4$  A, however, the  $\Psi(I)$  characteristic has a much greater gradient (see Fig. 40).

Figure 41 shows the inductance of the orthogonal pre-magnetization at a frequency of 100 kHz. In comparison to Fig. 36, no local maximum can be seen. The inductance is successively reduced by increasing the main current. Only from a main current of 75 mA, the inductance be slightly increased again by the auxiliary current. P, PM, PS or RM cores are particularly suitable for orthogonal pre-magnetization, since no hole must be drilled in these core forms. The hole is already in the center leg and is

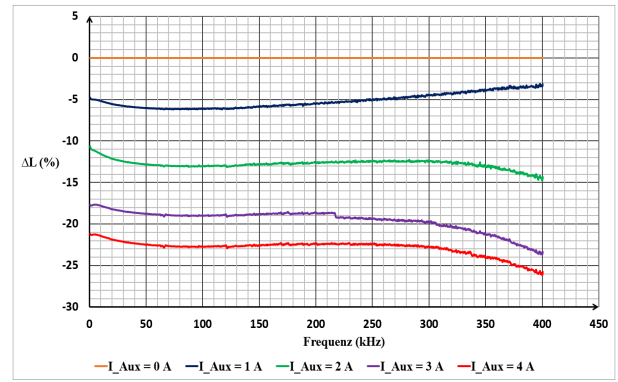


FIGURE 39. Measurement results of small-signal measurements at orthogonal biasing and  $I_1 = 0$  A.

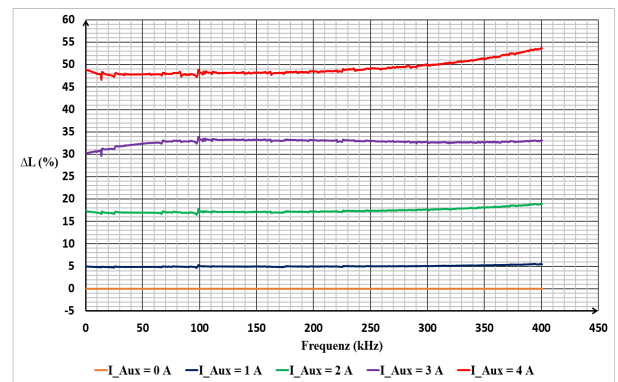


FIGURE 40. Measurement results of small-signal measurements at orthogonal biasing and  $I_1 = 1$  A.

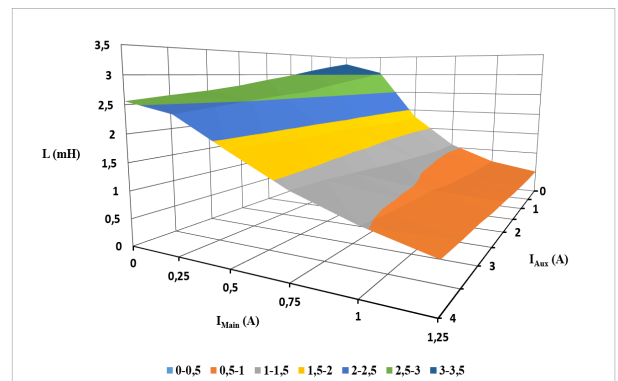


FIGURE 41. Inductance depending on  $I_1$  and  $I_{aux}$  at orthogonal biasing ( $f = 100$  kHz).

primarily used for mounting or air gap adjustment, but can be misused for pre-magnetization. The advantage of this variant is the saving of cost-intensive special ultrasonic drilling due to the brittle properties of ferrites. The disadvantage, however, is that only one hole is available and therefore very high currents are required to saturate the central core section. Figure 42 shows the results of a measurement on a P36/20 core, shown in Fig. 43, with an air gap of 85  $\mu$ m.

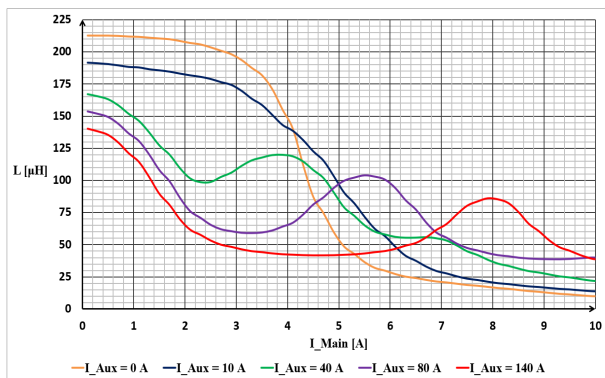


FIGURE 42. Measurement results of L-I-curves at orthogonal biasing of the P36/20 core ( $f = 10$  kHz).

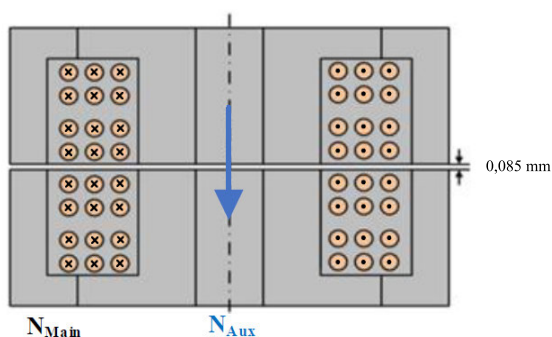


FIGURE 43. P36/20 core with an air gap of  $85 \mu\text{m}$ .

The measurement is again a small-signal measurement, where the frequency is not increased during the measurement, but the main current  $I_1$ . The measurement is carried out with the Wayne Kerr 3260B measuring instrument, using a sinusoidal measuring current with an effective value of 10 mA. In addition, a frequency of 10 kHz is selected, and automatic series of measurements are carried out at increasing main current  $I_1$  with preset current  $I_{aux}$ .

For an auxiliary current  $I_{aux} = 10$  A, the result corresponds to a purely orthogonal premagnetization as expected according to Fig. 38. For increasing auxiliary currents, however, the curve shape no longer corresponds to a purely orthogonal bias, but rather takes the form of the mixed bias magnetization curves. The magnetization characteristic curve from an auxiliary current  $I_{aux} = 80$  A corresponds more to a double S curve as shown in Fig. 30. The reason is that with these high auxiliary currents, a strong mixed premagnetization is noticeable in the upper and lower area of the center leg due to the high field strengths that arise.

#### D. DISCUSSION OF MEASUREMENTS

The measurements and evaluations of these tests require some preliminary considerations, since due to the transformer design, elements of the electric circuit for premagnetization are often also measured. In the measurement results shown here, care was taken to ensure that no influence is caused

by the additional circuits. The influences were eliminated accordingly by comparative measurements and calculations, so that errors could be minimized. Furthermore, the influence of parasitic capacitances and coupling capacitances, especially in small-signal measurements, cannot be neglected. However, false measurement results are not only caused by the influence of the test setup or the environment, but also by the measurement methodology. For small-signal measurements, either a fixed alternate voltage or an alternate current is specified, while the frequency or the main current  $I_1$  is successively increased during the measurement. The phase between current and voltage and, depending on the previous setting of alternate voltage or current (drive level), its counterpart is measured. The example of measurement via frequency illustrates the problem. In the lower frequency range, the impedance of an inductance is very low and thus, with the alternate voltage set, the resulting current is very high. In contrast, at high frequencies, the impedance is high and thus the resulting current is significantly lower. As a result, a measurement over the frequency produces a significantly different level of the hysteresis curve, which in turn has a significant effect on the inductance due to the non-linearity. Furthermore, the waveforms shown and thus also the control characteristics are significantly dependent on the selected alternate voltage waveform. In the tests shown, a pure sine-wave voltage was always used, which was repeatedly checked. Distortions of the voltages are directly visible in the inductance due to the changed hysteresis loop.

#### E. SUMMARY

The measurements have shown that there are several other ways to control an inductor in addition to the classical magnetic amplifier with an additional winding on the core. Not only the physical relationship of the windings to each other is crucial, but also the interconnection of the windings on a core plays a significant role (see Fig. 25 and 27). Furthermore, the core plays a decisive role in mixed and orthogonal premagnetization. Particularly in orthogonal premagnetization, areas are repeatedly created in which the fields in the core are no longer just orthogonal to each other despite the orthogonal arrangement of the windings. The effect is accordingly a transition to the magnetization characteristics of the mixed premagnetization (see Fig. 42). A further decisive influence for an application is the arrangement of the holes in the core. A comparison of Fig. 41 and 42 shows clearly that much higher currents with slightly fewer turns are necessary to achieve corresponding results.

In conclusion, it should be mentioned that a controllable magnetic component can be constructed using all three variants. A decisive difference between the mixed and orthogonal premagnetization through holes compared to the parallel biasing is that these types give the component completely new magnetization curves and thus properties. Parallel premagnetization, on the other hand, shifts the operating point on the original magnetization characteristic curve and thus exploits the nonlinear properties of the component.

## VI. POTENTIALS AND OPEN RESEARCH QUESTIONS

Through superimposition of differently aligned magnetic fields, an additional degree of freedom in the design process of magnetic devices is gained. This offers new possibilities and potentials for the overall application, regarding its design, control structure and efficiency.

As it was shown in Sec. II, some methods of superposing differently aligned magnetic fields have been used for decades. Other methods are still unused so far, which has various reasons. In this section, the potential of the presented methods in Sec. II will be addressed and discussed.

Furthermore, there are numerous open research questions which have to be investigated to get a deeper understanding of the technique.

### A. POTENTIALS

According to Sec. II, parallel biasing is often used, especially for variable inductors and transformers (see [18]–[22]) or in LED supply and general electronic ballast applications, as it is presented in [35]–[44].

However, mixed biasing as well as orthogonal biasing are rarely used nowadays. One important reason is the focus on semiconductor power devices, which have been subject to a rapid development over the last decades.

Controllable magnetic devices are able to support that improvement, e. g. through the achievement of zero-voltage switching (ZVS) which becomes more and more significant regarding the efficiency and cooling management of wide-band gap semiconductors, especially gallium nitride (GaN) devices.

An example for weight reduction of an inductor together with a reduction of switching losses using mixed and orthogonal biasing is presented in [119]. In this article, silicon (Si) MOSFETs are used for low voltage calculations, simulations and measurement results. Nevertheless, the approach is transferable to the GaN technology. Furthermore, the presented calculations and simulations for high voltage are performed using silicon carbide (SiC) MOSFETs. The results show a significant benefit in weight and efficiency for higher voltages because of the elimination of recovery losses.

To increase the efficiency of the auxiliary current circuit, the auxiliary winding can be applied with multiple turns. The required current decreases by the number of turns with no additional negative impact on the magnetic device as [121] shows.

Other investigations deal with harmonic mitigation using controllable magnetic devices. In [71], the concept of a VAG-VR is presented and investigated. This reactor makes use of mixed biasing, what requires additional drill holes within the iron core. The presented results show significant reductions of the 3rd as well as the 5th and 7th harmonic.

The concept has been developed through several prototypes (see [2]) and applied in a demonstrator for reactive power management in distribution grids

(medium-voltage grids) to compensate reactive power feed-in of renewable energy sources (see [121]).

Superimposition of differently aligned magnetic fields can be used to control resonant circuits and transformers. The variation of the transformers' main or leakage inductance could be used in resonant circuits to enable an operation on a fixed frequency, even with a variable load. In this design scenario, the needed auxiliary current in the transformer would replace the frequency as the main control parameter. A control structure for the auxiliary bias current would be more complicated than a frequency-based approach but the change could have a significant benefit on the application's characteristic regarding its electromagnetic compatibility.

### B. OPEN RESEARCH QUESTIONS

Although, superimposition of differently aligned magnetic fields in inductors and transformers has been used for almost a century and was subject of many investigations, there are still open research questions which will be dealt with within the following paragraphs.

An important question is the impact of the magnetic core's geometry on the behavior of the superposition. Especially regarding orthogonal biasing, it seems that the impact of the superimposition method depends on the core geometry. Further investigations have to be made to get a deeper understanding of the relations and inner processes within the core material.

A related question to the impact of the core geometry is the effect on the core losses. This question is particularly relevant to mixed and orthogonal biasing which tend to saturate main parts of the magnetic core material.

Core losses themselves are still a current research topic. Considering the permanent improvement and generalization of the Steinmetz equation, many impact factors have to be investigated. Furthermore, most investigations are limited to sinusoidal wave forms and small-signal measurements. There are some publications which deal with large-signal investigations, e. g. [123], but significantly more research is needed to obtain clarity related to core losses - with and without superimposed magnetic fields.

When referring to large-signal measurements, it has to be said that this topic also contains various open research questions. Especially regarding non-sinusoidal wave forms, only a few investigations have been made so far. Most investigations and publications rely on small-signal measurements made with sinusoidal wave forms. However, the bias point and with it the core magnetization is completely different compared to an application. The impact of these significant changes have to be investigated closely to optimize the magnetic device as well as the superimposition method.

In addition to the poor understanding of orthogonal flux interaction, there are currently no methods to analytically or numerically divide mixed interaction into parallel and orthogonal, though this aspect may gain significance with future better understanding of both single phenomena.

A large portion of the magnetic core is usually used for the magnetic circuit around the RSI resulting in high material consumption and ultimately high cost. Therefore, new core geometries as well as concepts to efficiently use existing ones must be developed.

As elaborated in Sec. III-B, the current models for orthogonal magnetization (and therefore mixed, too) rely on many, in part unrealistic assumptions, demanding better models. However, with more accurate intrinsic models, the existing theories for electric terminal behavior may quickly become powerful tools.

## VII. CONCLUSION

In this article, three different methods of flux interaction of differently aligned magnetic fields were presented. An overview of their history and usage as well as a mathematical modeling approach were given and discussed. The effects of the three methods were shown in simulation and measurement results. Furthermore, some possible applications were given and their potential was discussed.

The three different methods of flux interaction of differently aligned magnetic fields (parallel, mixed and orthogonal biasing) differ significantly in their mode of action and their applications. With their usage, an additional degree of freedom is gained during the device's design process that can create some significant benefits.

Furthermore, it has been shown that flux interaction can be represented within magnetic circuits, which again can be coupled with electric circuits. Parallel magnetization is as simple as adding another MMF source to the circuit and possibly to reluctances for a more realistic model. Orthogonal flux interaction is more complicated to describe as it needs the introduction of two or more nonlinearly coupled reluctances. The analytical and rather idealized theory to describe this coupling has been derived, assumptions have been identified and deviations have been estimated from realities. However, there is still a need for more profound theory, especially when it comes to intrinsic interaction on the microscopic scale. Also, specialized core geometries have to be invented in order to use orthogonal magnetization efficiently.

However, regardless of its possible potential, the majority of these methods is still unused to a large extent. The reasons might be the various open research questions. Further investigations are absolutely necessary and essential to unfold the possibilities that lie dormant in this technique.

## ACKNOWLEDGMENT

The authors thank the SUMIDA Components and Modules GmbH in Oberzell, Germany, for manufacturing or machining most of the ferrite cores which were used to generate the presented measurement results. Responsibility for the contents of this publication lies with the authors.

## REFERENCES

- [1] S. Lin, J. Friebe, S. Langfermann, and M. Owzareck, "Premagnetization of high-power low-frequency DC-inductors in power electronic applications," presented at the PCIM Eur., May 2019. [Online]. Available: <https://ieeexplore.ieee.org/document/8767669>
- [2] P. Zacharias, T. Kleeb, F. Fenske, J. Wende, and J. Pfeiffer, "Controlled magnetic devices in power electronic applications," presented at the EPE ECCE Eur., Sep. 2017. [Online]. Available: <https://ieeexplore.ieee.org/document/8099004>
- [3] J. Friebe, "Permanentmagnetische Vormagnetisierung von Speicherdrosseln in Stromrichtern," Ph.D. dissertation, Dept. Elect. Eng., Univ. Kassel, Kassel, Germany, 2014. [Online]. Available: <https://www.upress.uni-kassel.de/katalog/abstract.php?978-3-86219-820-7>
- [4] M. S. Perdigao, M. Menke, A. R. Seidel, R. A. Pinto, and J. M. Alonso, "A review on variable inductors and variable transformers: Applications to lighting drivers," presented at the IEEE Ind. Appl. Soc. Annu. Meeting, Oct. 2014. [Online]. Available: <https://ieeexplore.ieee.org/document/6978431>
- [5] E. F. W. Alexanderson, and S. P. Nixdorff, "A magnetic amplifier for radio telephony," *Proc. IRE*, vol. 4, no. 2, pp. 101–120, Apr. 1916. [Online]. Available: <https://ieeexplore.ieee.org/document/1645957>
- [6] C. Lufcy, "A survey of magnetic amplifiers," *Proc. IRE*, vol. 43, no. 4, pp. 404–413, 1955. [Online]. Available: <https://ieeexplore.ieee.org/document/4055426>
- [7] A. U. Lamm, "Some fundamentals of a theory of the transductor or magnetic amplifier," *Trans. Amer. Inst. Electr. Eng.*, vol. 66, no. 1, pp. 1078–1085, Jan. 1947. [Online]. Available: <https://ieeexplore.ieee.org/document/5059546>
- [8] F. Butcher and R. Willheim, "Some aspects of magnetic amplifier technique," *Proc. IRE*, vol. 40, no. 3, pp. 261–270, Mar. 1952. [Online]. Available: <https://ieeexplore.ieee.org/document/4050937>
- [9] D. W. V. Planck, L. A. Finzi, and D. C. Beaumariage, "Analytical determination of characteristics of magnetic amplifiers with feedback," *Trans. Amer. Inst. Electr. Eng.*, vol. 68, no. 1, pp. 565–570, Jul. 1949. [Online]. Available: <https://ieeexplore.ieee.org/document/5059976>
- [10] D. W. Ver Planck, M. Fishman, and D. C. Beaumariage, "An analysis of magnetic amplifiers with feedback," *Proc. IRE*, vol. 37, no. 8, pp. 862–866, Aug. 1949. [Online]. Available: <https://ieeexplore.ieee.org/document/1698102>
- [11] L. W. Buechler, "Magnetic amplifiers for naval shipboard applications," *Trans. Amer. Inst. Electr. Eng.*, vol. 67, no. 2, pp. 1241–1246, Jan. 1948. [Online]. Available: <https://ieeexplore.ieee.org/document/5059809>
- [12] T. R. Specht and R. N. Wagner, "The theory of the current transductor and its application in the aluminum industry," *Trans. Amer. Inst. Electr. Eng.*, vol. 69, no. 1, pp. 441–452, Jan. 1950. [Online]. Available: <https://ieeexplore.ieee.org/document/5060168>
- [13] W. A. Geyger, "Application of magnetic amplifiers in industrial instrumentation and control," *IRE Trans. Ind. Electron.*, vols. PGIE-5, no. 0, pp. 23–36, Apr. 1958. <https://ieeexplore.ieee.org/document/5007802>
- [14] R. E. Morgan, H. M. Ogle, and V. J. Wattenberger, "The extension of amplistat performance by A-C components," *Trans. Amer. Inst. Electr. Eng.*, vol. 69, no. 2, pp. 986–991, Jan. 1950. [Online]. Available: <https://ieeexplore.ieee.org/document/5060252>
- [15] H. Lehmann, "Predetermination of control characteristics of half-wave self-saturated magnetic amplifiers," *Trans. Amer. Inst. Electr. Eng.*, vol. 70, no. 2, pp. 2097–2103, Jul. 1951. [Online]. Available: <https://ieeexplore.ieee.org/document/5060682>
- [16] S. Cuk and Z. Zhang, "Coupled-inductor analysis and design," presented at the PESC, Jun. 1986. [Online]. Available: <https://ieeexplore.ieee.org/document/7415621>
- [17] D. Medini and S. S. Ben-Yaakov, "A current-controlled variable-inductor for high frequency resonant power circuits," presented at the APEC, Feb. 1994. [Online]. Available: <https://ieeexplore.ieee.org/document/316396>
- [18] M. S. Perdigao, B. Baptista, J. M. Alonso, and E. S. Saraiva, "Magnetic regulator topologies for dimmable electronic ballasts," presented at the ISIE, Jul. 2010. [Online]. Available: <https://ieeexplore.ieee.org/document/5637141>
- [19] M. Pajnić, P. Pejović, and O. Aleksić, "Design and analysis of a novel coupled inductor structure with variable coupling coefficient," *IET Power Electron.*, vol. 11, no. 6, pp. 961–967, May 2018. [Online]. Available: <https://ieeexplore.ieee.org/document/8358996>
- [20] Y. Hu, L. Huber, and M. M. Jovanović, "Single-stage, universal-input AC/DC LED driver with current-controlled variable PFC boost inductor," *IEEE Trans. Power Electron.*, vol. 27, no. 3, pp. 1579–1588, Mar. 2012. [Online]. Available: <https://ieeexplore.ieee.org/document/5593888>

- [21] E. A. Bitencourt, M. R. Cosetin, I. G. Vegner, and R. N. do Prado, "A ferromagnetic based variable inductor analysis and design methodology," presented at the COBEP/SPEC, Dec. 2015. [Online]. Available: <https://ieeexplore.ieee.org/document/7420081>
- [22] M. S. Perdigao, J. M. Alonso, D. G. Vaquero, and E. S. Saraiva, "Magnetically controlled electronic ballasts with isolated output: The variable transformer solution," *IEEE Trans. Ind. Electron.*, vol. 58, no. 9, pp. 4117–4129, Sep. 2011. [Online]. Available: <https://ieeexplore.ieee.org/document/5675678>
- [23] J. L. Vollin, F. D. Tan, and S. Cuk, "Magnetic regulator modeling," presented at the APEC, Mar. 1993. [Online]. Available: <https://ieeexplore.ieee.org/document/290727>
- [24] A. S. Kislovski, "Relative incremental permeability of soft ferrites as a function of the magnetic field H: An analytic approximation," presented at the PESC, May 1996. [Online]. Available: <https://ieeexplore.ieee.org/document/548775>
- [25] S. Saeed, J. Garcia, and R. Georgious, "Modeling of variable magnetic elements including hysteresis and Eddy current losses," presented at the APEC, Mar. 2018. [Online]. Available: <https://ieeexplore.ieee.org/document/8341254>
- [26] M. S. Perdigao, E. S. Saraiva, J. M. Alonso, and M. Cervi, "The controllable non-linear reactor in electronic ballasts applications: A behavioral analysis of the inductance as a function of both ac and DC bias currents," presented at the UPEC, Sep. 2008. [Online]. Available: <https://ieeexplore.ieee.org/document/4651669>
- [27] M. S. Perdigao, S. F. Ferreira, M. Martins, A. S. Mendes, and J. M. Alonso, "Finite element analysis of a variable inductor for an RSCC based LED lamp driver," presented at the IAS, Oct. 2015. [Online]. Available: <https://ieeexplore.ieee.org/document/7356874>
- [28] M. S. Perdigao, E. S. Saraiva, J. M. Alonso, and M. A. D. Costa, "Comparative analysis and experiments of resonant tanks for magnetically-controlled electronic ballasts," presented at the ISIE, May 2007. [Online]. Available: <https://ieeexplore.ieee.org/document/4375100>
- [29] J. M. Alonso, M. S. Perdigao, D. G. Vaquero, A. J. Calleja, and E. S. Saraiva, "Analysis, design, and experimentation on constant-frequency DC-DC resonant converters with magnetic control," *IEEE Trans. Power Electron.*, vol. 27, no. 3, pp. 1369–1382, Mar. 2012. [Online]. Available: <https://ieeexplore.ieee.org/document/5986725>
- [30] D. Zhang and J. Fletcher, "Modeling a DC-current-controlled variable inductance and its application to grid-tied converters," Presented at the POWERCON, Sep. 2016. [Online]. Available: <https://ieeexplore.ieee.org/document/7754075>
- [31] J. M. Alonso, G. Martinez, M. Perdigao, M. R. Cosetin, and R. N. do Prado, "A systematic approach to modeling complex magnetic devices using SPICE: Application to variable inductors," *IEEE Trans. Power Electron.*, vol. 31, no. 11, pp. 7735–7746, Nov. 2016. [Online]. Available: <https://ieeexplore.ieee.org/document/7478135>
- [32] J. M. Alonso, G. Martinez, M. Perdigao, M. Cosetin, and R. N. do Prado, "Modeling magnetic devices using SPICE: Application to variable inductors," Presented at the APEC, Mar. 2016. [Online]. Available: <https://ieeexplore.ieee.org/document/7468010>
- [33] J. M. Alonso, M. S. Perdigao, G. Z. Abdelmessih, M. A. D. Costa, and Y. Wang, "SPICE-aided design of a variable inductor in LED driver applications," presented at the IAS, Oct. 2016. [Online]. Available: <https://ieeexplore.ieee.org/document/7731895>
- [34] M. J. Alonso, S. M. Perdigao, Z. G. Abdelmessih, A. M. D. Costa, and Y. Wang, "SPICE modeling of variable inductors and its application to dingle inductor LED driver design," *IEEE Trans. Ind. Electron.*, vol. 64, no. 7, pp. 5894–5903, Jul. 2017. [Online]. Available: <https://ieeexplore.ieee.org/document/7781624>
- [35] B. Siegger, H. Guldner, and G. Hirschmann, "Ignition concepts for high frequency operated HID lamps," presented at the PESC, Jun. 2005. [Online]. Available: <https://ieeexplore.ieee.org/document/1581829>
- [36] Y. Hu, L. Huber, and M. M. Jovanovic, "Universal-input single-stage PFC flyback with variable boost inductance for high-brightness LED applications," presented at the APEC, Feb. 2010. [Online]. Available: <https://ieeexplore.ieee.org/document/5433669>
- [37] H. V. Marques, A. R. Seidel, M. S. Perdigao, J. M. Alonso, and E. S. Saraiva, "Development of a universal electronic ballast for TL5 lamps using a magnetic regulator," presented at the IAS, Oct. 2011. [Online]. Available: <https://ieeexplore.ieee.org/document/6074371>
- [38] H. V. Marques, A. R. Seidel, M. S. Perdigao, J. M. Alonso, and E. S. Saraiva, "Constant-frequency magnetically controlled universal ballast with SoS compliance for TL5 fluorescent lamps," *IEEE Trans. Power Electron.*, vol. 27, no. 4, pp. 2163–2175, Apr. 2012. [Online]. Available: <https://ieeexplore.ieee.org/document/5986726>
- [39] M. J. Alonso, S. M. Perdigao, A. D. Cota, and G. Martinez, "Analysis and experiments on a single-inductor half-bridge LED driver with magnetic control," *IEEE Trans. Power Electron.*, vol. 32, no. 12, pp. 9179–9190, Dec. 2017. [Online]. Available: <https://ieeexplore.ieee.org/document/7815409>
- [40] S. Borekci, "Dimming electronic ballasts without striations," *IEEE Trans. Ind. Electron.*, vol. 56, no. 7, pp. 2464–2468, Jul. 2009. [Online]. Available: <https://ieeexplore.ieee.org/document/4808132>
- [41] J. M. Alonso, M. A. Dalla Costa, M. Rico-Secades, J. Cardesin, and J. Garcia, "Investigation of a new control strategy for electronic ballasts based on variable inductor," *IEEE Trans. Ind. Electron.*, vol. 55, no. 1, pp. 3–10, Jan. 2008. [Online]. Available: <https://ieeexplore.ieee.org/document/4418511>
- [42] M. S. Perdigao, J. M. Alonso, M. A. D. Costa, and E. S. Saraiva, "Optimization of universal ballasts through magnetic regulators," presented at the APEC, Feb. 2008. [Online]. Available: <https://ieeexplore.ieee.org/document/4522877>
- [43] M. S. Perdigao, J. M. Alonso, M. A. D. Costa, and E. S. Saraiva, "Using magnetic regulators for the optimization of universal ballasts," *IEEE Trans. Power Electron.*, vol. 23, no. 6, pp. 3126–3134, Nov. 2008. [Online]. Available: <https://ieeexplore.ieee.org/document/4712527>
- [44] J. M. Alonso, M. S. Perdigao, J. Ribas, D. Gacio, and E. S. Saraiva, "A digitally-controlled universal ballast based on magnetic regulator and PSoC device," presented at the ISIE, Jul. 2009. [Online]. Available: <https://ieeexplore.ieee.org/document/5215663>
- [45] M. Gulko, D. Medini, and S. S. Ben-Yaakov, "Inductor-controlled current-sourcing resonant inverter and its application as a high pressure discharge lamp driver," presented at the APEC, Feb. 1994. [Online]. Available: <https://ieeexplore.ieee.org/document/316366>
- [46] S. V. Mollov and M. P. Theodoridis, "A comparison and optimum design of reluctance-controlled classical load-resonant converters," presented at the EPE PEMC, Sep. 2008. [Online]. Available: <https://ieeexplore.ieee.org/document/4635290>
- [47] G. Steiner, H. Zangl, P. Fulmek, and G. Brasseur, "A tuning transformer for the automatic adjustment of resonant loop antennas in RFID systems," presented at the ICIT, Dec. 2004. [Online]. Available: <https://ieeexplore.ieee.org/document/1490196>
- [48] S. Ben-Yaakov and M. M. Peretz, "A self-adjusting sinusoidal power source suitable for driving capacitive loads," *IEEE Trans. Power Electron.*, vol. 21, no. 4, pp. 890–898, Jul. 2006. [Online]. Available: <https://ieeexplore.ieee.org/document/7869727>
- [49] E. Orietti, P. Mattavelli, G. Spiazzi, C. Adragna, and G. Gattavari, "Two-phase interleaved LLC resonant converter with current-controlled inductor," presented at the COBEP, Sep. 2009. [Online]. Available: <https://ieeexplore.ieee.org/document/5347671>
- [50] D. R. Nayanasiiri, D. M. Vilathgamuwa, and D. L. Maskell, "Current-controlled resonant circuit based photovoltaic micro-inverter with half-wave cycloconverter," presented at the IAS, Oct. 2013. [Online]. Available: <https://ieeexplore.ieee.org/document/66824764>
- [51] Y. Jeong, G.-W. Moon, and J. Kim, "Analysis on half-bridge LLC resonant converter by using variable inductance for high efficiency and power density server power supply," presented at the APEC, Mar. 2017. [Online]. Available: <https://ieeexplore.ieee.org/document/7930689>
- [52] H. Fan and H. Li, "A novel phase-shift bidirectional DC-DC converter with an extended high-efficiency range for 20 kVA solid state transformer," presented at the ECCE, Sep. 2010. [Online]. Available: <https://ieeexplore.ieee.org/document/5617771>
- [53] H. Fan and H. Li, "High-frequency transformer isolated bidirectional DC-DC converter modules with high efficiency over wide load range for 20 kVA solid-state transformer," *IEEE Trans. Power Electron.*, vol. 26, no. 12, pp. 3599–3608, Dec. 2011. [Online]. Available: <https://ieeexplore.ieee.org/document/5934423>
- [54] S. M. Ahsanuzzaman, T. McRae, M. M. Peretz, and A. Prodic, "Low-volume buck converter with adaptive inductor core biasing," presented at the APEC, Feb. 2012. [Online]. Available: <https://ieeexplore.ieee.org/document/6165840>

- [55] F. Sichirollo, J. M. Alonso, and G. Spiazzi, "Use of current controlled mutual inductor to limit recycling current in the AHB-Flyback converter," presented at the IECON, Oct. 2012. [Online]. Available: <https://ieeexplore.ieee.org/document/6389504>
- [56] M. Beraki, M. S. Perdigao, F. Machado, and J. P. Trovao, "Auxiliary converter for variable inductor control in a DC-DC converter application," presented at the UPEC, Sep. 2016. [Online]. Available: <https://ieeexplore.ieee.org/document/8114107>
- [57] S. Saeed and J. Garcia, "Extended operational range of dual-active-bridge converters by using variable magnetic devices," presented at the APEC, Mar. 2019. [Online]. Available: <https://ieeexplore.ieee.org/document/8721920>
- [58] M. Pajnic and P. Pejovic, "Zero-voltage switching control of an interleaved bi-directional Buck-Boost converter with variable coupled inductor," *IEEE Trans. Power Electron.*, vol. 34, no. 10, pp. 9562–9572, Oct. 2019. [Online]. Available: <https://ieeexplore.ieee.org/document/8616867>
- [59] C.-Y. Lim, J.-H. Kim, Y. Jeong, D.-K. Kim, H.-S. Youn, and G. W. Moon, "A high efficiency critical mode boost PFC using a variable inductor," presented at the IPEMC ECCE Asia, May 2016. [Online]. Available: <https://ieeexplore.ieee.org/document/7512740>
- [60] T. Sasatani, Y. Narusue, Y. Kawahara, and T. Asami, "DC-based impedance tuning method using magnetic saturation for wireless power transfer," presented at the WPTC, May 2017. [Online]. Available: <https://ieeexplore.ieee.org/document/7953900>
- [61] J. E. Poniatowski and J. W. Walkinshaw, "Stacked variable inductor," U.S. Patent 7242275 B2, Jul. 10, 2007. [Online]. Available: <https://patents.google.com/patent/US7242275>
- [62] Y. Hu, L. Huber, and M. Jovanovic, "Current-controlled variable inductor," U.S. Patent 2011 248 812 A1, Oct. 13, 2011. [Online]. Available: <https://patents.google.com/patent/US20110248812A1/en>
- [63] B. Schneider and T. Uhl, "Inductive assembly," U.S. Patent 2 357 657 A3, Sep. 24, 2014. [Online]. Available: <https://patents.google.com/patent/EP2357657A3/en>
- [64] J. M. Alonso, M. A. D. Cota, J. Cardesin, J. Garcia, and M. Rico-Secades, "A new control method for electronic ballasts based on magnetic regulators," presented at the IAS, Oct. 2005. [Online]. Available: <https://ieeexplore.ieee.org/document/1518716>
- [65] J. M. Alonso, M. S. Perdigao, D. Gacio, L. Campa, and E. S. Saraiva, "Achieving constant frequency operation in DC-DC resonant converters through magnetic control," presented at the ECCE, Sep. 2010. [Online]. Available: <https://ieeexplore.ieee.org/document/5618109>
- [66] J. M. Alonso, M. S. Perdigao, J. Ribas, D. Gacio, and E. S. Saraiva, "Optimizing universal ballasts using magnetic regulators and digital control," *IEEE Trans. Ind. Electron.*, vol. 58, no. 7, pp. 2860–2871, Jul. 2011. [Online]. Available: <https://ieeexplore.ieee.org/document/5575415>
- [67] S. Zheng, J. Wang, F. Yang, F. Wang, L. M. Tolbert, and D. J. Costinett, "A DC controller for continuous variable series reactors CVSRs," presented at the ECCE, Sep. 2015. [Online]. Available: <https://ieeexplore.ieee.org/document/7310472>
- [68] K.-H. Park, Y. J. Choi, S. Choi, and D. Kim, "A novel adaptive magnetizing inductance control scheme for high-efficiency LLC resonant converter for PV applications," presented at the EPE ECCE Eur., Sep. 2015. [Online]. Available: <https://ieeexplore.ieee.org/document/7309275>
- [69] J. Kan, Y. Wu, Y. Tang, S. Xie, and L. Jiang, "Hybrid control scheme for photovoltaic microinverter with adaptive inductor," *IEEE Trans. Power Electron.*, vol. 34, no. 9, pp. 8762–8774, Sep. 2019. [Online]. Available: <https://ieeexplore.ieee.org/document/8556060>
- [70] Z. Zhao, W. Lu, W. Chen, X. Du, and H. Ho-Ching Iu, "Multi-period frame transient switching control for low-voltage high-current buck converter with a controlled coupled inductor," *IEEE Trans. Power Electron.*, vol. 34, no. 10, pp. 9743–9757, Oct. 2019. [Online]. Available: <https://ieeexplore.ieee.org/document/8598940>
- [71] S. L. Dolan, "Modelling and performance evaluation of the virtual air gap variable reactor," Ph.D. dissertation, Grad. Dept. Elect. and Comp. Eng., Univ. Toronto, Toronto, ON, Canada, 2009. [Online]. Available: <https://tspace.library.utoronto.ca/handle/1807/17754>
- [72] V. Molcrette, J.-L. Kotny, J.-P. Swan, and J.-F. Brudny, "Reduction of inrush current in single-phase transformer using virtual air gap technique," *IEEE Trans. Magn.*, vol. 34, no. 4, pp. 1192–1194, Jul. 1998. [Online]. Available: <https://ieeexplore.ieee.org/document/706479>
- [73] D. S. L. Dolan and P. W. Lehn, "Analysis of a virtual air gap variable reactor," presented at the PESC, Jun. 2007. [Online]. Available: <https://ieeexplore.ieee.org/document/4342160>
- [74] J. Avila-Montes and E. Melgoza, "Scaling the virtual air-gap principle to high voltage large power applications," presented at the ICEIMach, Sep. 2012. [Online]. Available: <https://ieeexplore.ieee.org/document/6349960>
- [75] E. Melgoza, J. Avila-Montes, and M. Madrigal, "Analysis of the magnetic characteristics of virtual-gap reactors," presented at the ROPEC, Nov. 2013. [Online]. Available: <https://ieeexplore.ieee.org/document/6702731>
- [76] A. Konrad and J. F. Brudny, "An improved method for virtual air gap length computation," *IEEE Trans. Magn.*, vol. 41, no. 10, pp. 4051–4053, Oct. 2005. [Online]. Available: <https://ieeexplore.ieee.org/document/1519532>
- [77] A. Konrad and J. F. Brudny, "Virtual air gap length computation with the finite-element method," *IEEE Trans. Magn.*, vol. 43, no. 4, pp. 1829–1832, Apr. 2007. [Online]. Available: <https://ieeexplore.ieee.org/document/4137764>
- [78] D. S. L. Dolan and P. W. Lehn, "Finite element analysis of a virtual air gap variable transformer," presented at the CCECE, May 2008. [Online]. Available: <https://ieeexplore.ieee.org/document/4564664>
- [79] A. A. Abrishami and H. Heydari, "Improved accuracy for finite element modeling in virtual air gap length computation," presented at the IEEEIC, May 2014. [Online]. Available: <https://ieeexplore.ieee.org/document/6835877>
- [80] J.-F. Brudny, G. Parent, and I. Naceur, "Characterization and modeling of a virtual air gap by means of a reluctance network," *IEEE Trans. Magn.*, vol. 53, no. 7, Jul. 2017, Art. no. 8002007. [Online]. Available: <https://ieeexplore.ieee.org/document/7875149>
- [81] S. Magdaleno and C. P. Rojas, "Control of the magnetizing characteristics of a toroidal core using virtual gap," presented at the CERMA, Oct. 2010. [Online]. Available: <https://ieeexplore.ieee.org/document/5692393>
- [82] Y. Zhang, R. A. Dougal, and H. Zheng, "Tieline reconnection of microgrids using controllable variable reactors," presented at the IAS, Oct. 2013. [Online]. Available: <https://ieeexplore.ieee.org/document/6682489>
- [83] Y. Zhang, P. Devakota, and R. Fu, "Analysis on practical design of virtual-air-gap variable reactors for tieline reclosing in micro-grid," presented at the ECCE, Sep. 2014. [Online]. Available: <https://ieeexplore.ieee.org/document/6953662>
- [84] Y. Zhang, R. Shrestha, and R. Fu, "Enabling fail-safe and initial charge limitation in uncontrolled rectifiers by applying virtual-air-gap variable reactors," presented at the ICPE ECCE Asia, Jun. 2015. [Online]. Available: <https://ieeexplore.ieee.org/document/7168095>
- [85] J. Avila-Montes, D. Campos-Gaona, E. Melgoza Vazquez, and J. R. Rodriguez-Rodriguez, "A novel compensation scheme based on a virtual air gap variable reactor for AC voltage control," *IEEE Trans. Ind. Electron.*, vol. 61, no. 12, pp. 6547–6555, Dec. 2014. [Online]. Available: <https://ieeexplore.ieee.org/document/6809145>
- [86] V. Majchrzak, G. Parent, J. Brudny, V. Costan, and P. Guinic, "Coupling transformer with a virtual air gap for the protection of dynamic voltage restorers," presented at the IECON, Oct. 2014. [Online]. Available: <https://ieeexplore.ieee.org/document/7048541>
- [87] E. Haugs and F. Strand, "Controllable transformer," U.S. Patent 2 467 989 C, Apr. 24, 2012. [Online]. Available: <https://patents.google.com/patent/CA2467989C/en>
- [88] J. Brudny, P. Guinic, and V. Costan, "Series current limiter using a magnetic circuit comprising holes and windows," U.S. Patent 2012 126 886 A1, Sep. 27, 2012. [Online]. Available: <https://patents.google.com/patent/WO2012126886A1/en>
- [89] P. Guinic, J. Brudny, V. Costan, and M. Dessoude, "Series voltage regulator with electronics protected against short-circuits by magnetic circuit-based decoupling using holes and windows," U.S. Patent 2 686 746 B1, Apr. 22, 2015. [Online]. Available: <https://patents.google.com/patent/EP2686746B1/en>
- [90] D. S. L. Dolan and P. W. Lehn, "Harmonic mitigation in a virtual air gap variable reactor via control current modulation," presented at the PES, Jul. 2008. [Online]. Available: <https://ieeexplore.ieee.org/document/4595983>
- [91] D. S. L. Dolan, P. W. Lehn, and T. Taufik, "Harmonics and dynamic response of a virtual air gap variable reactor," presented at the ITNG, Apr. 2012. [Online]. Available: <https://ieeexplore.ieee.org/document/6209150>
- [92] S. E. Tez, "The parametric transformer," Ph.D. dissertation, Dept. Electron. Elect. Eng., Loughborough Univ., Loughborough, U.K., 2009. [Online]. Available: [https://repository.lboro.ac.uk/articles/The\\_parametric\\_transformer/9520040](https://repository.lboro.ac.uk/articles/The_parametric_transformer/9520040)

- [93] R. Verma and W. Fam, "Theory and performance of parametric transformers," *IEEE Trans. Power App. Syst.*, vols. PAS-91, no. 6, pp. 2494–2504, Nov. 1972. [Online]. Available: <https://ieeexplore.ieee.org/document/4075018>
- [94] E. S. Tez and I. R. Smith, "Energy-transfer mechanism and current waveforms of parametric transformers," *IEE Proc. B Electr. Power Appl.*, vol. 130, no. 3, pp. 181–185, May 1983. [Online]. Available: <https://ieeexplore.ieee.org/document/4643617>
- [95] E. S. Tez and I. R. Smith, "The parametric transformer: A power conversion device demonstrating the principles of parametric excitation," *IEEE Trans. Educ.*, vol. 27, no. 2, pp. 56–65, May 1984. [Online]. Available: <https://ieeexplore.ieee.org/document/4321665>
- [96] W. Fam and G. Bahl, "Two related types of parametric transformers," *IEEE Trans. Magn.*, vol. 10, no. 3, pp. 690–693, Sep. 1974. [Online]. Available: <https://ieeexplore.ieee.org/document/1058372>
- [97] H. Oka and P. P. Biringer, "Flux control and flux distribution in a ferrite orthogonal core," *IEEE Trans. Magn.*, vol. 25, no. 5, pp. 3839–3841, Sep. 1989. [Online]. Available: <https://ieeexplore.ieee.org/document/42450>
- [98] H. Hong, J. Zhang, M. Song, W. Gong, K. Cao, Y. Sun, J. Cui, D. Wang, Q. Li, B. Tian, Z. Wei, N. Zou, Z. Xiong, B. Shu, and Y. Xin, "Magnetization study on a new type of orthogonally configured magnetic core structure and its potential application to superconducting controllable reactors," *IEEE Trans. Appl. Supercond.*, vol. 23, no. 3, Jun. 2013, Art. no. 5001004. [Online]. Available: <https://ieeexplore.ieee.org/document/6491454>
- [99] Z. H. Meiksin, "Comparison of orthogonal and parallel-flux variable inductors," *IEEE Trans. Ind. Appl.*, vols. IA-10, no. 3, pp. 417–423, May 1974. [Online]. Available: <https://ieeexplore.ieee.org/document/4157612>
- [100] W. Fam and I. Khan, "Steady-state analysis of parametric frequency changers," *IEEE Trans. Magn.*, vol. 13, no. 4, pp. 1070–1075, Jul. 1977. [Online]. Available: <https://ieeexplore.ieee.org/document/1059510>
- [101] O. Ichinokura and K. Murakami, "Graphical circuit analysis of two C-core type parametric power converter," *IEEE Trans. Magn.*, vol. 14, no. 5, pp. 1002–1004, Sep. 1978. [Online]. Available: <https://ieeexplore.ieee.org/document/1059982>
- [102] P. K. Sen and W. Z. Fam, "Analysis of the parametric converter," *IEEE Trans. Ind. Electron. Control Instrum.*, vols. IECL-26, no. 2, pp. 93–98, May 1979. [Online]. Available: <https://ieeexplore.ieee.org/document/1059982>
- [103] K. Tajima, A. Kaga, Y. Anazawa, and O. Ichinokura, "One method for calculating flux-MMF relationship of orthogonal-core," *IEEE Trans. Magn.*, vol. 29, no. 6, pp. 3219–3221, Nov. 1993. [Online]. Available: <https://ieeexplore.ieee.org/document/281142>
- [104] K. Tajima, A. Kaga, and O. Ichinokura, "Transient analysis of a push-pull parametric transformer at start-up time," *IEEE Trans. Magn.*, vol. 33, no. 5, pp. 3334–3336, Sep. 1997. [Online]. Available: <https://ieeexplore.ieee.org/document/617935>
- [105] O. Ichinokura, K. Tajima, and K. Murakami, "An analysis of orthogonal-core type push-pull parametric transformer with nonlinear load," *IEEE Transl. J. Magn. Jpn.*, vol. 5, no. 8, pp. 655–661, Aug. 1990. [Online]. Available: <https://ieeexplore.ieee.org/document/4564315>
- [106] O. Ichinokura, K. Tajima, and T. Jinzenji, "Analysis of parametric transformer with rectifier load," *IEEE Transl. J. Magn. Jpn.*, vol. 8, no. 3, pp. 156–160, Mar. 1993. [Online]. Available: <https://ieeexplore.ieee.org/document/4565596>
- [107] W. Z. Fam and P. K. Sen, "The operation of a parametric transformer between two busbars," *IEEE Trans. Power App. Syst.*, vol. 94, no. 3, pp. 858–865, May 1975. [Online]. Available: <https://ieeexplore.ieee.org/document/1601518>
- [108] W. Fam and A. Goel, "Thyristor control of parametric transformers," *IEEE Trans. Magn.*, vol. 16, no. 5, pp. 925–927, Sep. 1980. [Online]. Available: <https://ieeexplore.ieee.org/document/1060816>
- [109] K. Murakami, S. Kikuchi, and T. Watanabe, "Characteristics of a new AC motor making good use of parametric oscillation," *IEEE Trans. Magn.*, vol. 16, no. 5, pp. 931–933, Sep. 1980. [Online]. Available: <https://ieeexplore.ieee.org/document/1060673>
- [110] O. Ichinokura, S. Kikuchi, and K. Murakami, "A new AC power stabilizer using two-orthogonal-flux type parametric transformer and variable inductor," *IEEE Trans. Magn.*, vol. 18, no. 6, pp. 1761–1763, Nov. 1982. [Online]. Available: <https://ieeexplore.ieee.org/document/1062198>
- [111] O. Ichinokura, M. Maeda, H. Takahashi, and K. Murakami, "A new orthogonal-core type DC-AC converter for photovoltaic power system," *IEEE Trans. Magn.*, vol. 24, no. 2, pp. 1969–1971, Mar. 1988. [Online]. Available: <https://ieeexplore.ieee.org/document/11662>
- [112] O. Ichinokura, K. Tajima, and T. Jinzenji, "Study of push-pull parametric transformer," *IEEE Trans. Magn.*, vol. 28, no. 5, pp. 2181–2183, Sep. 1992. [Online]. Available: <https://ieeexplore.ieee.org/document/179436>
- [113] Y. Ishigaki, M. Hosoya, M. Yasumura, and H. Sakamoto, "Applications of the cross transformer," *IEEE Trans. Consum. Electron.*, vols. CE-28, no. 3, pp. 305–320, Aug. 1982. [Online]. Available: <https://ieeexplore.ieee.org/document/4179971>
- [114] H. Oka and P. P. Biringer, "Control characteristic analysis of a ferrite orthogonal core," *IEEE Trans. Magn.*, vol. 26, no. 5, pp. 2888–2893, Sep. 1990. [Online]. Available: <https://ieeexplore.ieee.org/document/104902>
- [115] O. Ichinokura, T. Kagami, T. Jinzenji, M. Maeda, and Y. Wakiya, "High speed variable-inductor controlled with DC-DC converter," *IEEE Trans. Magn.*, vol. 31, no. 6, pp. 4247–4249, Nov. 1995. [Online]. Available: <https://ieeexplore.ieee.org/document/489941>
- [116] E. S. Kuh and I. N. Hajj, "Nonlinear circuit theory: Resistive networks," *Proc. IEEE*, vol. 59, no. 3, pp. 340–355, Mar. 1971. [Online]. Available: <https://ieeexplore.ieee.org/document/1450106>
- [117] A. N. Willson, "Some aspects of the theory of nonlinear networks," *Proc. IEEE*, vol. 61, no. 8, pp. 1092–1113, Aug. 1973. [Online]. Available: <https://ieeexplore.ieee.org/document/1451143>
- [118] E. M. I. Schulz, "Modellierung der orthogonalen magnetisierung auf basis empirischer materialuntersuchungen," M.S. thesis, Inst. Drive Syst. Power Electron., Gottfried Wilhelm Leibniz Universität Hannover, Hannover, Germany, 2020. [Online]. Available: <https://www.repo.uni-hannover.de/handle/123456789/10136>
- [119] D. Eichhorst, J. Pfeiffer, and P. Zacharias, "Weight reduction of DC/DC converters using controllable inductors," presented at the PCIM Eur., May 2019. [Online]. Available: <https://ieeexplore.ieee.org/document/8767714>
- [120] P. Zacharias, *Magnetische Bauelemente*. Wiesbaden, Germany: Springer, 2020. [Online]. Available: <https://link.springer.com/book/10.1007/978-3-658-24742-3>
- [121] J. Pfeiffer, P. Küster, Y. Erenler, Z. H. S. Qashlan, and P. Zacharias, "Impact of implementation of auxiliary bias-windings on controllable inductors for power electronic converters," presented at the EPE ECCE Eur., Sep. 2020. [Online]. Available: <https://ieeexplore.ieee.org/document/9215616>
- [122] F. Fenske, M. Faßhauer, and P. Zacharias, "Neuartige robuste Stellglieder zum Blindleistungsmanagement in Verteilnetzen (NR2-RPC)," Dept. Elect. Power Eng., Univ. Kassel, Kassel, Germany, Tech. Rep., to be published.
- [123] A. Stadler, "Messtechnische bestimmung und simulation der kernverluste in weichmagnetischen materialien," Ph.D. dissertation, Dept. Elect., Electron. Commun. Eng., Friedrich-Alexander Univ. Erlangen-Nürnberg, Erlangen, Germany, 2009.



**JONAS PFEIFFER** (Member, IEEE) received the Diploma and M.Sc. degrees in electrical engineering from the University of Kassel, Germany, where he is currently pursuing the Dr.Ing. degree in electrical engineering with the Department of Electrical Power Engineering, with a focus on passive components and controllable magnetic devices.



**PIERRE KÜSTER** was born in Alsfeld, Hessen, Germany, in 1993. He received the B.Sc. and M.Sc. degrees from the University of Kassel, Germany, in 2017 and 2018, respectively, with a focus on electrical energy systems, where he is currently pursuing the Ph.D. degree in electrical engineering. Since 2018, he has been a Research Assistant of KDEE-EVS with the University of Kassel. His research interest includes the further development of magnetics for power electronics.



**ILKA E. M. SCHULZ** is currently pursuing the degree in electrical engineering with Leibniz University Hannover, with a focus on passive components in power electronics and orthogonal magnetization. Since 2018, she has been working as a Student Assistant with the Institute for Drive and Power Electronics, Leibniz University Hannover.



**JENS FRIEBE** (Member, IEEE) was born in Göttingen, Germany. He received the B.Sc., M.Sc., and Dr.Ing. degrees in electrical engineering from the University of Kassel, Germany. He is responsible for the research area of passive components in power electronics with the Institute for Drive Systems and Power Electronics, Leibniz University Hannover, Germany, since January 2018. Before that, he has worked for more than 13 years at SMA Solar Technology, Germany, in the field of

PV-Inverter topologies, wide-bandgap semiconductors, magnetic components, control strategies for high-switching frequencies, and power electronics packaging. He invented more than 30 granted patents in the field of power electronics.



**PETER ZACHARIAS** (Member, IEEE) received the Dipl.Ing. and the Dr.Ing. degrees in electrical engineering from the “Otto-von-Guericke” University Magdeburg, Germany, in 1979 and 1981, respectively. He has worked with the University of Magdeburg, until 1990, as an Associate Professor for power electronics with the research fields of power electronics for high-voltage applications and pulsed power. From 1990 to 1995, he has worked with Lambda Physik Goettingen. From 1995 to 2001, he was with the Institute for Solar Energy Technology (ISET), Kassel. In 2001, he changed to eupec/Infineon in Warstein. Since 2005, he has been active as a Full Professor for electric power supply systems at the University of Kassel. Since January 2009, he has been the Head of the Centre of Competence for Distributed Electric Power Supply Systems (KDEE). His major research interests include power electronic converters for public power supply.

...